Photoinduced Electron Transfer in Amino Acid Assemblies

Sandra L. Mecklenburg, Brian M. Peek, Jon R. Schoonover, Dewey G. McCafferty, Craig G. Wall, Bruce W. Erickson,* and Thomas J. Meyer*

Contribution from the Department of Chemistry, University of North Carolina, Chapel Hill, North Carolina 27599-3290

Received November 3, 1992

Abstract: The preparation and photophysical characterization of a series of redox-active lysines and related model compounds based on polypyridyl ruthenium complexes are described. Donor–chromophore–acceptor triad **1**, [PTZpn-Lys($Ru^{II}b_2m$)$^{2+}$-NH-prPQ^{2+}]$(PF_6^-)_4$ (see below), was prepared by assembly of a modified ruthenium bipyridyl chromophore ($Ru^{II}b_2m$, where b = 2,2′-bipyridine, m = 4′-methyl-2,2′-bipyridyl-4′-carbonyl), an electron donor (phenothiazine, PTZ), and an electron acceptor (paraquat, PQ^{2+}) on a lysine (Lys) scaffold utilizing amide bonds. This derivatized amino acid exhibited efficient (>95%) quenching of the ruthenium metal-to-ligand charge-transfer (MLCT) excited state upon irradiation with a 420-nm laser pulse in CH_3CN. The resulting redox-separated state, [(PTZpn$^{\bullet+}$)-Lys($Ru^{II}b_2m$)$^{2+}$-NH-(prPQ$^{\bullet+}$)], stored 1.17 eV and lived for 108 ns ($k = 9.26 \times 10^6$ s^{-1}) as observed by transient absorption spectroscopy. Also studied was a series of related model systems that included model chromophores, simple chromophore-quencher dyads linked by amide bonds, and chromophore-quencher dyads based on lysine. An account of the kinetic behavior of these systems including triad **1** and a discussion of factors that influence the lifetime of the redox-separated states, their efficiency of formation, and their energy storage ability are presented.

Introduction

In a preliminary account, the photophysical properties of the synthetic trifunctional amino acid [PTZpn-Lys($Ru^{II}b_2m$)$^{2+}$-NH-prPQ^{2+}] (**1**) were described.[1,2] Following MLCT excitation of

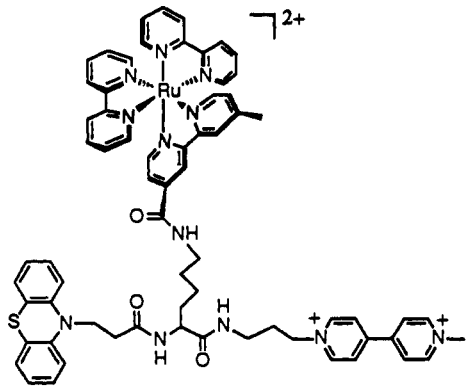

1 PTZpn-Lys($Ru^{II}b_2m$)$^{2+}$-NH-prPQ^{2+}

this donor–chromophore–acceptor (DCA) triad, a series of electron transfer events led to formation of a redox-separated state (RSS).

$$\text{PTZpn-Lys}(Ru^{II}b_2m)^{2+}\text{-NH-prPQ}^{2+} \xrightarrow[CH_3CN]{h\nu_{420nm}} \text{PTZpn}^{\bullet+}\text{-Lys}(Ru^{II}b_2m)^{2+}\text{-NH-prPQ}^{\bullet+} \quad (1)$$

This assembly represents an addition to a class of donor–chromophore–acceptor molecules that mimic natural photosynthetic reaction centers in yielding separated redox equivalents as a result of free-energy gradients. Other assemblies in this class include carotenoid porphyrin-quinones,[3] aniline porphyrin-quinones,[4] and ruthenium–polypyridyl complexes.[5]

The key feature in the construction of the amino acid assembly **1** was the application of a modular approach based on well-established amino acid coupling chemistry, which has been employed in the preparation of other molecules used to study the effects of distance and orientation in electron and energy transfer.[6-8] We designed and prepared carboxylic acid or amino derivatives of donors, chromophores, and acceptors suitable for condensation with each other and with amino acids through formation of amide bonds. In this way, a large number of synthetic targets can be addressed by combining various redox-active modules.

This report documents the preparations and characterizations of the lysine-based triad **1** and relevant model compounds, describes in detail their photophysical properties as studied by

(1) Mecklenburg, S. L.; Peek, B. M.; Erickson, B. W.; Meyer, T. J. *J. Am. Chem. Soc.* **1991**, *113*, 8540.

(2) Abbreviations: bpy or b = 2,2′-bipyridine; Boc = *tert*-butoxycarbonyl; BQ = 1,4-benzoquinone; Lys = L-lysine; m = 4′-methyl-2,2′-bipyridine-4-carbonyl; PTZ = 10*H*-phenothiazine; PTZpn = 3-(10*H*-phenothiazine-10)-propanoyl; PQ^{2+} = paraquat (1,1′-dimethyl-4,4′-bipyridinium); $prPQ^{2+}$ = 3-(1′-methyl-4,4′-bipyridinium)propyl; and TMBD = *N,N,N′,N′*-tetramethylbenzidine.

(3) (a) Gust, D.; Moore, T. A.; Moore, A. L.; et al. *J. Am. Chem. Soc.* **1991**, *113*, 3638. (b) Gust, D.; Moore, T. A.; Moore, A. L.; Lee, S.-J.; Bittersmann, E.; Luttrull, D. K.; Rehms, A. A.; DeGraziano, J. M.; Ma, X. C.; Gao, F.; Belford, R. E.; Trier, T. T. *Science* **1990**, *248*, 199. (c) Gust, D.; Moore, T. A. *Science* **1989**, *244*, 35. (d) Gust, D.; Moore, T. A.; Moore, A. L.; Makings, L. R.; Seely, G. R.; Ma, X.; Trier, T. T.; Gao, F. *J. Am. Chem. Soc.* **1988**, *110*, 7567. (e) Moore, T. A.; Gust, D.; Mathis, P.; Mialocq, J.-C.; Chachaty, C.; Bennsasson, R. V.; Band, E. J.; Doizi, D.; Liddell, P. A.; Lehman, W. R.; Nemeth, G. A.; Moore, A. L. *Nature* **1984**, *307*, 630.

(4) (a) Wasielewski, M. R.; Gaines, G. L., III; O'Neil, M. P.; Svec, W. A.; Niemczyk, M. P. *J. Am. Chem. Soc.* **1990**, *112*, 4559. (b) Hofstra, U.; Schaafsma, T. J.; Sanders, G. M.; Van Dijk, M.; Van Der Plas, H. C.; Johnson, D. G.; Wasielewski, M. R. *Chem. Phys. Lett.* **1988**, *151*, 169. (c) Schmidt, J. A.; McIntosh, A. R.; Weedon, A. C.; Bolton, J. R.; Connolly, J. S.; Hurley, J. K.; Wasielewski, M. R. *J. Am. Chem. Soc.* **1988**, *110*, 1733. (d) Wasielewski, M. R.; Niemczyk, M. P.; Svec, W.; Pewitt, E. B. *J. Am. Chem. Soc.* **1985**, *107*, 5562.

(5) (a) Jones, W. E., Jr.; Bignozzi, C. A.; Chen, P.; Meyer, T. J. *Inorg. Chem.* **1993**, *32*, 1167. (b) Worl, L. A.; Strouse, G. F.; Younathan, J. N.; Baxter, S. M.; Meyer, T. J. *J. Am. Chem. Soc.* **1990**, *112*, 7571. (c) Meyer, T. J. *Acc. Chem. Res.* **1989**, *22*, 163. (d) Strouse, G. F.; Worl, L. A.; Younathan, J. N.; Meyer, T. J. *J. Am. Chem. Soc.* **1989**, *111*, 9101. (e) Danielson, E.; Elliott, C. M.; Merkert, J. W.; Meyer, T. J. *J. Am. Chem. Soc.* **1987**, *109*, 2519. (f) Olmsted, J., III; McClanahan, S. F.; Danielson, E.; Younathan, J. N.; Meyer, T. J. *J. Am. Chem. Soc.* **1987**, *109*, 3297. (g) Margerum, L. D.; Murray, R. W.; Meyer, T. J. *J. Phys. Chem.* **1986**, *90*, 728.

(6) (a) Inai, Y.; Sisido, M.; Imanishi, Y. *J. Phys. Chem.* **1991**, *95*, 3847. (b) Sisido, M.; Tanaka, R.; Inai, Y.; Imanishi, Y. *J. Am. Chem. Soc.* **1989**, *111*, 6790.

(7) Schanze, K. S.; Sauer, K. *J. Am. Chem. Soc.* **1988**, *110*, 1180.

(8) (a) Vassilian, A.; Wishart, J. F.; van Hemelryck, B.; Schwarz, H.; Isied, S. S. *J. Am. Chem. Soc.* **1990**, *112*, 7278. (b) Isied, S. S.; Vassilian, A.; Magnuson, R. H.; Schwarz, H. A. *J. Am. Chem. Soc.* **1985**, *107*, 7432.

0002-7863/93/1515-5479$04.00/0

transient laser spectroscopy, and provides an account of the photophysical events that occur in these systems following photoexcitation of the chromophore.

Experimental Section

Materials. The following salts were prepared and purified as described previously:[9] 4′-methyl-2,2′-bipyridine-4-carboxylic acid, m-OH, **2**; bis(2,2′-bipyridine)(4′-methyl-2,2′-bipyridine-4-carboxamidomethane)ruthenium(II) bis(hexafluorophosphate), $[(Ru^{II}b_2m\text{-}NHCH_3)^{2+}](PF_6^-)_2$, **3**; N^{α}-(1,1-dimethylethoxycarbonyl)-N^{ϵ}-(bis(2,2′-bipyridine)(4′-methyl-2,2′-bipyridine-4-carbonyl)ruthenium(II))-L-lysine bis(hexafluorophosphate), $[Boc\text{-}Lys(Ru^{II}b_2m)^{2+}\text{-}OH](PF_6^-)_2$, **4**; N^{α}-(bis(2,2′-bipyridine)(4′-methyl-2,2′-bipyridine-4-carbonyl)ruthenium(II))-L-alanyl-N^{ϵ}-(3-(10*H*-phenothiazine-10)propanoyl)-L-lysyl-L-alanine bis(hexafluorophosphate), $[(Ru^{II}b_2m)^{2+}\text{-}Ala\text{-}Lys(PTZpn)\text{-}Ala\text{-}OH](PF_6^-)_2$, **7**.

***N*-Methyl-4′-methyl-2,2′-bipyridine-4-carboxamide, [m-NHCH$_3$].** *N*-Methylmorpholine (NMM, 3.0 equiv, 1.4 mmol), methylamine hydrochloride (1.5 equiv, 0.70 mmol, dried 6 h under vacuum), and (1-benzotriazoleoxy)tris(pyrrolidino)phosphonium PF_6^- (PyBOP, 1.2 equiv, 0.29 g) were added successively to a solution of m-OH (100 mg, 0.47 mmol) in dry *N*,*N*-dimethylformamide (DMF, 4 mL). A $CaSO_4$ drying tube was installed, and the reaction was stirred overnight. The solvent was removed under high vacuum (0.2 Torr) overnight. The residue was dissolved in ethyl acetate (25 mL) and extracted with 5% $NaHCO_3$ (4 × 25 mL). The organic phase was dried over Na_2SO_4, decanted, and evaporated to give a white solid, which was recrystallized from acetone to give m-$NHCH_3$ (40 mg, 36% yield) as white crystals: ^{1}H NMR ($CDCl_3$, 400 MHz) δ 2.35 (s, 3 H, 4′-CH_3), 2.93 (d, J = 4.5 Hz, 3 H, NH-CH_3), 7.08 (d, J = 4.6 Hz, 1 H, 5′), 7.46 (br s, 1 H, NH), 7.71 (d, J = 5.0 Hz, 1 H, 5), 8.15 (s, 1 H, 3′), 8.41 (d, J = 4.9 Hz, 1 H, 6′), 8.60 (s, 1 H, 3), and 8.66 ppm (d, J = 4.9 Hz, 1 H, 6).

Tris(4′-methyl-2,2′-bipyridine-4-carboxamidomethane)ruthenium(II) Bis(hexafluorophosphate), $[Ru^{II}(m\text{-}NHCH_3)_3^{2+}](PF_6^-)_2$. A black-green solution of $RuCl_3$ (1.0 equiv, 0.056 mmol, 11.5 mg) and m-$NHCH_3$ (3 equiv, 0.166 mmol, 40 mg) in DMF (1 mL) was stirred and heated at reflux. The appearance of the MLCT absorption of the title compound at 458 nm was followed by UV–visible spectroscopy. The reaction was monitored by ion-exchange HPLC and was complete after 2 h. Addition of saturated aqueous NH_4PF_6 gave a flocculent mud-brown precipitate, which was collected and dissolved in a large volume of acetone. The solution was filtered and freed of solvent under reduced pressure. The red-brown residue was dissolved in CH_2Cl_2 (10 mL) and extracted with aqueous NH_4PF_6 (3 × 10 mL). The organic layer was dried over Na_2SO_4, decanted, and evaporated. The crude product (25 mg) was purified by ion-exchange HPLC and precipitated as the PF_6^- salt, $[Ru^{II}(m\text{-}NHCH_3)_3^{2+}](PF_6^-)_2$, (40% yield): ^{1}H NMR (CD_3CN, 400 MHz) δ 2.54 (s, 9 H, 3 × 4′-CH_3), 2.91 (d, J = 4.7 Hz, 9 H, 3 × NH-CH_3), 7.26 (t, J = 6.2 Hz, 3 H, 3 × m5′), 7.36 (br s, 3 H, 3 × NH), 7.52 (m, 3 H, 3 × m5), 7.59 (t, J = 7.3 Hz, 3 H, 3 × m6′), 7.80 (d, J = 9.9 Hz, d, J = 5.6 Hz, 3 H, 3 × m6), 8.48 (s, 3 H, 3 × m3′), and 8.74 ppm (s, 3 H, 3 × m3).

3-(1′-Methyl-4,4′-bipyridinium)propylammonium Tris(hexafluorophosphate), $[NH_3^+\text{-}prPQ^{2+}](PF_6^-)_3$. Solid 3-bromopropylammonium bromide (4.0 g, 18.2 mmol) and 1-methyl-4-(4′-pyridyl)-pyridinium PF_6^- (1.91 g, 6.04 mmol) were dissolved with stirring in CH_3CN (61 mL), protected from light, and heated at reflux for 8 h. The resulting solid was collected by filtration and washed with hot CH_3CN (2 × 20 mL). The remaining solid was dissolved in a hot mixture of methanol (20 mL) and water (0.5 mL). Solid NH_4PF_6 (4 equiv) was added, and the solution was cooled to room temperature. Diethyl ether (14 mL) was added until a precipitate formed. The mixture was heated and just enough methanol was added to obtain a clear solution, which was cooled overnight at 5 °C. The resulting solid was collected by filtration to afford the pure title compound (1.3 g, 32% yield) as a white solid: UV (CH_3CN) λ (ϵ) 258 nm (23 500 L mol^{-1} cm^{-1}); FAB-MS (calcd for $C_{14}H_{20}F_{12}N_3P_2$ $[(M + 2PF_6)^+]$ m/z 520, calcd for $C_{14}H_{19}F_6N_3P$ $[(M + PF_6)^+]$ m/z 374, calcd for $C_{14}H_{19}N_3$ $[M^+]$ m/z 229) m/z 520, 374, and 229; ^{1}H NMR ($(CD_3)_2CO$) δ 2.36 (pentet, 2 H, 2pr-CH_2), 3.09 (t, J = 7.4 Hz, 2 H, 3pr-CH_2), 4.40 (s, 3 H, CH_3), 4.69 (t, J = 7.7 Hz, 2 H, 1pr-CH_2), 8.37 (d, J = 6.7 Hz, 2 H, 3′ & 5′), 8.43 (d, J = 6.9 Hz, 2 H, 3 & 5), 8.86 (d, J = 6.8 Hz, 2 H, 2′ & 6′), and 8.93 ppm (d, J = 7.1 Hz, 2 H, 2 & 6). Anal. Calcd for $C_{14}H_{20}F_{18}N_3P_3 + {}^1/_6NH_4PF_6$: C, 24.11; H, 2.99; N 6.37. Found: C, 23.98; H, 2.85; N, 6.32.

***N*-[3-(1′-Methyl-4,4′-bipyridinium)propyl]-3-(10*H*-Phenothiazine-10)propanamide Bis(hexafluorophosphate), $[PTZpn\text{-}NH\text{-}prPQ^{2+}](PF_6^-)_2$, 10.** 3-(10*H*-Phenothiazine-10)propanoic acid (PTZpn-OH, 49 mg, 0.18 mmol),[10] $[NH_3^+\text{-}prPQ^{2+}](PF_6^-)_3$ (100 mg, 0.15 mmol), and NMM (59 μL, 0.54 mmol) were dissolved in DMF (2.0 mL) and stirred at room temperature with exclusion of light. Solid PyBOP (94 mg, 0.18 mmol) was added, the flask was stoppered, the mixture was stirred overnight, and the solvent was removed by rotary evaporation. A solution of the resulting solid in a minimal amount of acetone (5.0 mL) was stirred as 20 mM aqueous NH_4PF_6 (120 mL) was added. The blue-black solid which formed was collected by filtration and dried under vacuum to afford the title dyad (99 mg, 85% yield). Part (15 mg) was dissolved in 2:3 (v/v) CH_3CN/0.6 mM phosphate buffer (pH 7.2, 4.0 mL) and purified by ion-exchange HPLC. Fractions containing the desired material were combined and CH_3CN was removed under vacuum. The aqueous residue was treated with 0.3 M NH_4PF_6 to precipitate a blue-black solid, which was collected by filtration and dried to afford pure $[PTZpn\text{-}NH\text{-}prPQ^{2+}](PF_6^-)_2$ (11 mg, 58% yield): UV (CH_3CN) λ (ϵ) 254 nm (25 400 L mol^{-1} cm^{-1}); FAB-MS (calcd for $C_{29}H_{30}F_{12}N_4OP_2S$ $[(M + 2PF_6)^+]$ m/z 772; calcd for $C_{29}H_{30}F_6N_4OPS$ $[(M + PF_6)^+]$ m/z 627; calcd for $C_{29}H_{30}N_4OS$ $[M^+]$ m/z 482) m/z 772, 627, and 482; ^{1}H NMR ($(CD_3)_2CO$) δ 2.35 (m, 2 H, CH_2), 2.72 (t, J = 6.6 Hz, 2 H, CH_2-CO), 3.34 (q, J = 6.6 Hz, 2 H, N^{pr}-C-CH_2), 4.33 (t, J = 6.5 Hz, 2 H, N^{PTZ}-CH_2), 4.74 (s, 3 H, N^{PQ}-CH_3), 4.90 (t, J = 6.7 Hz, 2 H, N^{PQ}-CH_2), 6.93–7.03 (m, 3 H, 2 × PTZ & N^{pr}H), 7.05–7.17 (m, 4 H, PTZ), 7.18–7.26 (m, 2 H, PTZ), 8.74–8.83 (m, 4 H, 3,3′,5,5′-PQ), and 9.37 ppm (d, J = 5.9 Hz, 4 H, 2,2′,6,6′-PQ).

***N*-(3-(1′-Methyl-4,4′-bipyridinium)propyl)bis(2,2′-bipyridine)-4′-methyl-2,2′-bipyridine-4-carboxamide)ruthenium(II) Bis(hexafluorophosphate), $[(Ru^{II}b_2m)^{2+}\text{-}NH\text{-}prPQ^{2+}](PF_6^-)_2$, 5.** (1-Benzotriazoleoxy)tris(dimethylamino)phosphonium hexafluorophosphate (BOP, 44 mg, 0.098 mmol) and diisopropylethylamine (DIEA, 0.037 g, 0.287 mmol) were added to a solution of $[(Ru^{II}b_2m)^{2+}\text{-}OH](PF_6^-)_2$ (75 mg, 0.082 mmol) and $[NH_3^+\text{-}prPQ^{2+}](PF_6^-)_3$ (55 mg, 0.082 mmol) in DMF (1.5 mL). After the reaction was stirred in the dark overnight, the DMF was removed under reduced pressure. The orange solid was suspended in phosphate buffer (pH 7, 6 mL) and kept overnight at 5 °C. The solid was collected and washed with water to afford the title compound (101 mg, 87% yield), which was purified further by ion-exchange HPLC: ^{1}H NMR (CD_3CN) δ 2.56 (s, 3 H, m-CH_3), 3.50 (pentet, 2 H, CH_2), 3.54 (q, J = 6.0 Hz, 2 H, N^{pr}-CH_2), 4.40 (s, 3 H, N^{PQ}-CH_3), 4.71 (t, J = 7.39 Hz, 2 H, N^{PQ}-CH_2), 8.39 (dd, 4 H, 3,3′,5,5′-PQ), 8.85 (d, J = 6.96 Hz, 2 H, 2′,6′-PQ), and 9.00 ppm (d, J = 6.43 Hz, 2 H, 2,6-PQ) plus the following b and m protons: 7.29 (dd, 1 H, m5′) 7.40 (t, 4 H, b5), 7.57 (d, J = 5.78, 1 H, m5), 7.70 (m, 5 H, b6, m6′), 7.88 (d, J = 5.96 Hz, 1 H, m6), 8.06 (t, 4 H, b4), 8.5 (d, 5 H, b3, m3′), and 8.82 ppm (s, 1 H, m3).

10-(3-Aminopropyl)-10*H*-phenothiazine Hydrochloride, [PTZpr-NH_2·HCl]. The amine hydrochloride was prepared by the method of Godefroi and Little.[11] 3-(10*H*-Phenothiazine-10)propionitrile[12] (5.06 g, 20 mmol) was placed in a Soxhlet extractor and extracted into diethyl ether (200 mL) containing 1.73 g (46 mmol) of lithium aluminum hydride. After 72 h excess hydride was decomposed by successive addition of water (1.7 mL), 20% aqueous NaOH (1.7 mL), and water (6.9 mL). The salts were removed by filtration, and HCl gas was bubbled into the ethereal filtrate to provide the title compound (4.70 g, 80% yield) as a light purple solid: mp 227.5–230.0 °C. An analytical sample of PTZprNH_2·HCl was obtained by recrystallization from 95% EtOH: mp 229.0–230.0 °C (lit.[11] 226–228 °C); MS (calcd for $C_{15}H_{16}N_2S$ $[MH^+]$: m/z 257) m/z 257; ^{1}H NMR ($(CD_3)_2SO$) δ 1.98 (t, $J_{2pr,3pr}$ = 7.4 Hz, t, $J_{1pr,2pr}$ = 7.0 Hz, 2 H, 2pr-CH_2), 2.86 (t, $J_{2pr,3pr}$ = 7.4 Hz, 2 H, 3pr-CH_2), 3.98 (t, $J_{1pr,2pr}$ = 7.0 Hz, 2 H, 1pr = CH_2-PTZ), 6.92–7.09 (m, 4 H, PTZ), 7.15–7.26 (m, 4 H, PTZ), and 8.08 ppm (br s, 3 H, NH_3). Anal. Calcd for $C_{15}H_{16}N_2S$·HCl: C, 61.53; H, 5.85; N, 9.57. Found: C, 61.64; H, 5.86; N, 9.61.

***N*-(3-(10*H*-Phenothiazine-10)propyl)-4′-methyl-2,2′-bipyridine-4-carboxamide, [m-NH-prPTZ].** A suspension of 4′-methyl-2,2′-bipyridine-4′-carboxylic acid[9b] (0.100 g, 0.47 mmol) in $SOCl_2$ (3.0 mL, 41.1 mmol) was heated at reflux until clear and yellow (20 min). Excess $SOCl_2$ was removed by rotary evaporation under high vacuum (0.25 Torr) to give 4′-methyl-2,2′-bipyridine-4-carbonyl chloride (m-Cl) as a yellow solid (0.110 g). It was dissolved in CH_2Cl_2 (30 mL) and used immediately. Light was excluded from the following steps at all times. PTZprNH_2·HCl (0.300 g, 1.02 mmol) was dissolved in 1 M Na_2CO_3 (10 mL) and extracted with CH_2Cl_2 (3 × 10 mL). The combined organic phase was dried over anhydrous Na_2SO_4, filtered, and added dropwise to the solution of m-Cl

(9) (a) Peek, B. M.; Ross, G. T.; Edwards, S. W.; Meyer, G. J.; Meyer, T. J.; Erickson, B. W. *Int. J. Peptide Protein Res.* **1991**, *38*, 114. (b) Peek, B. M. Ph.D. Dissertation, University of North Carolina at Chapel Hill, 1991.
(10) Cauquil, G.; Cassadevall, A. *C. R. Acad. Sci. Paris* **1947**, *225*, 578.
(11) Godefroi, E. F.; Little, E. L. *J. Org. Chem.* **1956**, *21*, 1163–1168.

in CH_2Cl_2 with stirring. During the addition, the solution turned dark pink and a light pink precipitate formed. The mixture was heated at reflux for 10 min, cooled to room temperature, and filtered to remove the precipitated PTZprNH$_2$·HCl. The filtrate was washed with 5% citric acid (3 × 30 mL), brine (3 × 30 mL), 1 M Na_2CO_3 (3 × 30 mL), and brine (3 × 30 mL), dried over anhydrous Na_2SO_4, filtered, and freed of solvent by rotary evaporation to furnish the title compound (0.162 g, 76% yield) as a rose-colored solid: mp 75.0–77.0 °C; MS (calcd for $C_{27}H_{25}N_4OS$ [MH$^+$]: *m/z* 452) *m/z* 452; ^{1}H NMR ($(CD_3)_2CO$) δ 2.19 (t, $J_{2pr,3pr}$ = 6.9 Hz, t, $J_{1pr,2pr}$ = 6.8 Hz, 2 H, 2pr-CH$_2$), 3.59–3.66 (m, 2 H, 1pr = CH$_2$-PTZ), 4.11 (t, $J_{2pr,3pr}$ = 6.9 Hz, 2 H, 3pr-CH$_2$), 6.93 (t *J* = 7.6 Hz, d, *J* = 1.0 Hz, 2 H, 3,6-PTZ), 7.07–7.23 (m, 6 H, PTZ), 7.32 (d, $J_{5',6'}$ = 4.5 Hz, 1 H, m5′), 7.77 (d, $J_{5,6}$ = 4.8 Hz, d, $J_{3,5}$ = 1.3 Hz, 1 H, m5), 8.36 (s, 1 H, m3′), 8.56 (d, $J_{5',6'}$ = 4.9 Hz, 1 H, m6′), 8.77 (d, $J_{5,6}$ = 5.0 Hz, 1 H, m6), and 8.87 ppm (s, 1 H, m3). Anal. Calcd for $C_{27}H_{25}N_4OS$: C, 71.50; H, 5.56; N, 12.35. Found: C, 71.43; H, 5.64; N, 12.27.

(*N*-(3-(10*H*-Phenothiazine-10)propyl)-4′-methyl-2,2′-bipyridine-4-carboxamide)(bis(2,2′-bipyridine)ruthenium(II)) Bis(hexafluorophosphate), [(Ru^{II}b$_2$m)$^{2+}$-NH-prPTZ](PF$_6^-$)$_2$, 6. Light was excluded from this reaction at all times. A suspension of solid Rub_2Cl_2 (0.050 g, 0.09 mmol) and solid m-NH-prPTZ (0.041 g, 0.09 mmol) in 70% ethanol (100 mL) was heated at reflux for 4.5 h and gradually turned orange and clear. The mixture was cooled to room temperature, and the ethanol was removed by rotary evaporation. Water (20 mL) was added and the suspension was filtered through a fine-porosity glass frit. Saturated NH_4PF_6 (3 mL) was added to the filtrate and the resulting orange precipitate was collected by filtration, washed with water (5 × 30 mL) and diethyl ether (5 × 30 mL), and dried under vacuum to afford an orange solid (84 mg). It was purified by cation-exchange chromatography on Sephadex CM-25 (Pharmacia) by successive elution with 0.01 M, 0.1 M, and 1 M aqueous NH_4Cl (500 mL each). Saturated NH_4PF_6 (3 mL) was added to the 100-mL fraction that contained the purified product as measured by HPLC. The resulting aqueous suspension was extracted with CH_2Cl_2 (3 × 20 mL). The combined organic phase was dried over anhydrous Na_2SO_4, filtered, and freed of solvent by rotary evaporation under high vacuum (0.25 Torr) to afford HPLC-pure [(Rub$_2$m)$^{2+}$-NH-prPTZ](PF$_6^-$)$_2$ (78 mg, 75% yield) as an orange solid: mp 185.0 °C dec; MS (calcd for $C_{47}H_{40}N_8OS\,P_2F_{12}Ru$ [MH$^+$] *m/z* 1150) *m/z* 1150, 453, 432, 257; ^{1}H NMR ($(CD_3)_2CO$) δ 2.13 (t, $J_{2pr,3pr}$ = 6.5 Hz, $J_{1pr,2pr}$ = 6.6 Hz, 2 H, 2pr-CH$_2$), 2.61 (s, 3 H, m-4-CH$_3$), 3.55–3.64 (m, 2 H, 1pr = CH$_2$-PTZ), 4.09 (t, *J* = 6.5 Hz, 2 H, 3pr-CH$_2$), 6.91 (t, *J* = 7.7 Hz, d, *J* = 1.3 Hz, 2 H, 3,6-PTZ), 7.01–7.07 (m, 4 H, 1,4,5,8-PTZ), 7.19 (t, *J* = 7.6 Hz, d, *J* = 1.6 Hz, 2 H, 2,7-PTZ), 7.51 (d, *J* = 4.7 Hz, 2 H, m5′), 7.54–7.66 (m, 4 H, 4 × b5), 7.75 (d, *J* = 5.5 Hz, d, *J* = 1.7 Hz, 1 H, m5), 7.85 (d, *J* = 5.8 Hz, 1 H, m6), 8.04–8.28 (m, 9 H, 4 × b4, 4 × b6, m6′), 8.74 (s, 1 H, m3′), 8.81–8.85 (m, 4 H, 4 × b3), and 8.94 ppm (s, 1 H, m3). Anal. Calcd for $C_{47}H_{40}N_8OS\,P_2F_{12}Ru{\cdot}2H_2O$: C, 47.72; H, 3.69; N, 9.29. Found: C, 47.56; H, 3.74; N, 9.44.

N$^{\alpha}$-(1,1-Dimethylethoxycarbonyl)-N$^{\epsilon}$-(bis(2,2′-bipyridine)(4′-methyl-2,2′-bipyridine-4-carbonyl)ruthenium(II))-L-lysine Methyl Ester Bis(hexafluorophosphate), [Boc-Lys(Ru^{II}b$_2$m)$^{2+}$-OCH$_3$](PF$_6^-$)$_2$. Boc-L-Lysine-OCH$_3$·HCl (Bachem, 0.312 g, 1.05 mmol), [(Ru^{II}b$_2$m-OH)$^{2+}$](PF$_6^-$)$_2$ (0.50 g, 0.54 mmol),[9a] NMM (0.244 mL, 2.22 mmol), and DMF (5.5 mL) were stirred at room temperature. Solid PyBOP (0.312 g, 0.60 mmol) was added, the flask was stoppered, and the mixture was stirred overnight. After the solvent was removed by rotary evaporation, the remaining dark red oil was dissolved in CH_2Cl_2 (50 mL). This solution was washed with 20 mM NH_4PF_6 (3 × 50 mL), dried over $MgSO_4$, filtered, and rotary evaporated to dryness. A solution of the remaining solid in a minimum amount of CH_3CN (3.0 mL) was added dropwise to rapidly stirring diethyl ether, which precipitated an orange solid. After the solution was cooled at 5 °C for 2 h, the solid was collected by filtration and dried under vacuum to afford [Boc-Lys(Ru^{II}b$_2$m)$^{2+}$-OCH$_3$]$^{2+}$(PF$_6^-$)$_2$ (0.563 g, 90% yield): UV–vis (CH_3CN) λ (ε) 246 (21 000), 288 (55 000), and 456 nm (11 600 L cm^{-1} mol^{-1}); FAB-MS (calcd for $C_{44}H_{48}N_8O_5Ru$ [M$^+$] *m/z* 870.2790) *m/z* 870.2827; ^{1}H NMR ($(CD_3)_2CO$) δ 1.37 (s, 9 H, $(CH_3)_3C$), 1.43–1.84 (m, 6 H, C$^{\beta}$H$_2$ & C$^{\gamma}$H$_2$ & C$^{\delta}$H$_2$), 2.60 (s, 3 H, m4′-CH$_3$), 3.39–3.48 (m, 2 H, C$^{\epsilon}$H$_2$), 3.66 (s, 3 H, OCH$_3$), 4.06–4.13 (m, 1 H, C$^{\alpha}$H), 6.21 (d, *J* = 8.46 Hz, 1 H, N$^{\alpha}$H), 7.45 (d, *J* = 4.9 Hz, 1 H, m5′), 7.53–7.62 (m, 4 H, b5), 7.84–7.91 (m, 2 H, m5 & m6′), 8.02–8.25 (m, 10 H, N$^{\epsilon}$H & m6 & 4 × (b4 & b6)), 8.80 (m, 5 H, m3′ & 4 × b3), and 9.03 ppm (br s, 1 H, m3).

N$^{\alpha}$-(3-(10*H*-Phenothiazine-10)propanoyl)-N$^{\epsilon}$-(bis(2,2′-bipyridine)(4′-methyl-2,2′-bipyridine-4-carbonyl)ruthenium(II))-L-lysine Methyl Ester Bis(hexafluorophosphate), [PTZpn-Lys(Ru^{II}b$_2$m)$^{2+}$-OCH$_3$](PF$_6^-$)$_2$, 8. [Boc-Lys(Ru^{II}b$_2$m)$^{2+}$-OCH$_3$](PF$_6^-$)$_2$ (200 mg, 0.17 mmol) was stirred in 4 N HCl/dioxane at 0 °C for 1 h. The solvent was removed by rotary evaporation to afford an oily orange solid, which was dried under vacuum overnight. Part (100 mg, 0.091 mmol) of this material, PTZpn-OH[9a] (38 mg, 0.14 mmol), and NMM (46 mL, 0.42 mmol) were dissolved in DMF (1.0 mL) with stirring. Solid PyBOP (72 mg, 0.14 mmol) was added, the flask was stoppered, the mixture was stirred overnight, and the solvent was removed by rotary evaporation. A solution of the residual orange solid in CH_3CN (1.5 mL) was added dropwise to rapidly stirring ethyl acetate. The orange precipitate was collected by filtration to afford the title dyad as an orange solid (62 mg). Part (20 mg) was dissolved in 2:3 (v/v) CH_3CN/0.6 mM phosphate buffer (pH 7.2, 4.0 mL) and purified by ion-exchange HPLC. Fractions containing the desired material were combined and the CH_3CN was removed under vacuum. The aqueous residue was treated with 0.3 M NH_4PF_6, which precipitated an orange solid. The solid was collected by filtration and dried to afford pure [PTZpn-Lys(Ru^{II}b$_2$m)$^{2+}$-OCH$_3$](PF$_6^-$)$_2$ (14 mg, 36% yield): UV–vis (CH_3CN) λ(ε) 254 (38 200), 288 (52 000) and 456 nm (11 600 Lmol^{-1} cm^{-1}), FAB-MS (calcd for $C_{54}H_{51}F_{12}N_9O_4P_2RuS$ [(M + 2PF$_6$)$^+$] *m/z* 1313; calcd for $C_{54}H_{51}N_9O_4PRuS$ [(M + PF$_6$)$^+$] *m/z* 1168; calcd for $C_{54}H_{51}N_9O_4RuS$ [M$^+$] *m/z* 1023) *m/z* 1313, 1168, and 1023; ^{1}H NMR ($(CD_3)_2CO$) δ 1.37–1.48 (m, 2 H, C$^{\delta}$H$_2$), 1.58–1.90 (m, 4 H, C$^{\beta}$H$_2$ & C$^{\gamma}$H$_2$), 2.59 (s, 3 H, m4′-CH$_3$), 2.74 (m, 2 H, CH$_2$-CO), 3.40 (m, 2 H, C$^{\epsilon}$H$_2$), 3.64 (s, 3 H, OCH$_3$), 4.20 (t, *J* = 6.3 Hz, 2 H, N^{PTZ}-CH$_2$), 4.41–4.52 (m, 1 H, C$^{\alpha}$H), 6.88–7.02 (m, 4 H, PTZ), 7.10–7.20 (m, 4 H, PTZ), 7.46–7.61 (m, 7 H, m5′ & m5 & N$^{\alpha}$H & 4 × b5), 7.84–7.90 (m, 2 H, m6′ & m6), 8.03–8.25 (m, 9 H, N$^{\epsilon}$H & 4 × (b6 & b4)), 8.79–8.84 (m, 5 H, m3′ & 4 × b3), and 9.05 ppm (br s, 1 H, m3).

N$^{\alpha}$-(1,1-Dimethylethoxycarbonyl)-N$^{\epsilon}$-(bis(2,2′-bipyridine)(4′-methyl-2,2′-bipyridine-4-carbonyl)ruthenium(II))-L-lysine 3-(1′-Methyl-4,4′-bipyridinium)propylamide Tetrakis(hexafluorophosphate), [Boc-Lys-(Ru^{II}b$_2$m)$^{2+}$-NH-prPQ^{2+}](PF$_6^-$)$_4$, 9. [Boc-Lys(Ru^{II}b$_2$m)$^{2+}$-OH](PF$_6^-$)$_2$ (102 mg, 0.087 mmol), [H$_3$N$^+$-prPQ^{2+}](PF$_6^-$)$_3$ (63.4 mg, 0.096 mmol), NMM (31.6 μL, 0.288 mmol), and DMF (1.0 mL) were stirred at room temperature. Solid PyBOP (50 mg, 96 μmol) was added, the flask was stoppered, and the mixture was stirred overnight. After the solvent was removed by rotary evaporation, the remaining orange solid was dissolved in 2:3 (v/v) CH_3CN/0.6 mM phosphate buffer (pH 7.2, 4.0 mL) and purified by ion-exchange HPLC. Fractions containing the desired material were combined, and the CH_3CN was removed under vacuum. The aqueous residue was treated with 0.3 M NH_4PF_6, which precipitated an orange solid. The solid was collected by filtration, dried under vacuum, suspended in 4:1 (v/v) acetone/CH_2Cl_2, and filtered to remove any salts that might have precipitated with the orange material. The solvent was removed to afford [Boc-Lys(Ru^{II}b$_2$m)$^{2+}$-NH-prPQ^{2+}](PF$_6^-$)$_4$ (111 mg, 78% yield) as an orange solid: UV–vis (CH_3CN) λ (ε) 254 (28 700), 288 (49 500), and 456 nm (10 000 L cm^{-1} mol^{-1}); FAB-MS (calcd for $C_{57}H_{63}F_{18}N_{11}O_4P_3Ru$ [(M + 3PF$_6$)$^+$] *m/z* 1502; calcd for $C_{57}H_{63}F_{12}N_{11}O_4P_2Ru$ [(M + 2PF$_6$)$^+$] *m/z* 1357; calcd for $C_{57}H_{63}F_6N_{11}O_4PRu$ [(M + PF$_6$)$^+$] *m/z* 1212) *m/z* 1502, 1357, and 1212; ^{1}H NMR ($(CD_3)_2CO$) δ 1.35–2.03 (m, 6 H, C$^{\beta}$H$_2$-C$^{\gamma}$H$_2$-C$^{\delta}$H$_2$), 1.39 (s, 9 H, $(CH_3)_3C$), 2.38–2.45 (m, 2 H, N^{pr}-C-CH$_2$), 2.60 (s, 3 H, m4′-CH$_3$), 3.32–3.51 (m, 4 H, C$^{\epsilon}$H$_2$ & N^{pr}-CH$_2$), 4.04–4.23 (m, 1 H, C$^{\alpha}$H), 4.74 (s, 3 H, N^{PQ}-CH$_3$), 4.97 (t, *J* = 6.6 Hz, 2 H, N^{PQ}-CH$_2$), 6.28 (d, *J* = 6.6 Hz, 1 H, N$^{\alpha}$H), 7.49 (d, *J* = 6.6 Hz, 1 H, m5′), 7.52–7.66 (m, 5 H, N^{PQ}H & 4 × b5), 7.85–7.89 (m, 2 H, m5 & m6′), 8.00–8.13 (m, 4 H, b4), 8.15–8.28 (m, 6 H, m6 & N$^{\epsilon}$H & 4 × b6), 8.77–8.89 (m, 9 H, 3,3′,5,5′-PQ & m3′ & 4 × b3), 9.09 (br s, 1 H, m3), 9.36 (d, *J* = 6.5 Hz, 2 H, 2′,6′-PQ), and 9.46 ppm (d, *J* = 6.3 Hz, 2 H, 2,6-PQ).

N$^{\alpha}$-(3-(10*H*-Phenothiazine-10)propanoyl)-N$^{\epsilon}$-(bis(2,2′-bipyridine)-(4′-methyl-2,2′-bipyridine-4-carbonyl)ruthenium(II))-L-lysine 3-(1′-Methyl-4,4′-bipyridinium)propylamide Tetrakis(hexafluorophosphate), [PTZ-pn-Lys(Ru^{II}b$_2$m)$^{2+}$-NH-prPQ^{2+}](PF$_6^-$)$_4$, 1. A suspension of [Boc-Lys-(Ru^{II}b$_2$m)$^{2+}$-prPQ^{2+}](PF$_6^-$)$_4$ (90 mg, 0.050 mmol) was stirred in 4 N HCl/dioxane at 0 °C for 1 h. The solvent was removed by rotary evaporation, and the orange solid residue was dried under vacuum overnight. This orange solid, PTZpn-OH[10] (19 mg, 0.071 mmol), and NMM (23.4 μL, 0.21 mmol) were dissolved in DMF (1.0 mL) with stirring. Solid PyBOP (37 mg, 0.071 mmol) was added, the flask was stoppered, and the mixture was stirred for 6 h at room temperature in the dark. After the solvent was removed by rotary evaporation, the dark red solid was dissolved in CH_3CN (2.0 mL). The solution was filtered and added dropwise to a rapidly stirring solution of 20 mM NH_4PF_6. The sticky orange solid which formed was collected by filtration, dissolved in CH_3CN (2.0 mL), and added dropwise to rapidly stirring diethyl ether. The solid which formed was collected by filtration to afford the desired product (82 mg, 91% yield). Part (21 mg) was dissolved in 2:3 (v/v) CH_3CN/0.6 mM phosphate buffer (pH 7.2, 4.0 mL) and purified by

ion-exchange HPLC. Fractions containing the desired material were combined, the CH_3CN was removed under vacuum, and the aqueous residue was treated with 0.3 M NH_4PF_6. The orange precipitate was collected by filtration and dried under vacuum to afford pure $[PTZpn\text{-}Lys(Ru^{II}b_2m)^{2+}\text{-}NH\text{-}prPQ^{2+}](PF_6^-)_4$ (13 mg, 56% yield): UV–vis (CH_3CN) λ (ϵ) 254 (51 200), 288 (56 800), 456 nm (11 700 L mol^{-1} cm^{-1}); FAB-MS (calcd for $C_{67}H_{66}F_{18}N_{12}O_3P_3RuS$ $[(M + 3PF_6)^+]$ m/z 1655; calcd for $C_{67}H_{66}F_{12}N_{12}O_3P_2RuS$ $[(M + 2PF_6)^+]$ m/z 1510; calcd for $C_{67}H_{66}F_6N_{12}O_3PRuS$ $[(M + PF_6)^+]$ m/z 1365) m/z 1655, 1510, and 1365; ^1H NMR (CD_3CN) δ 1.26–1.43 (m, 2 H, $C^\delta H_2$), 1.52–1.80 (m, 4 H, $C^\beta H_2$ & $C^\gamma H_2$), 1.96–2.08 (m, 2 H, CH_2), 2.54 (s, 3 H, m4′-CH_3), 2.72 (t, J = 6.3 Hz, 2 H, CH_2-CO), 3.11–3.28 (m, 2 H, N^{pr}-CH_2), 3.31–3.40 (m, 2 H, $C^\epsilon H_2$), 3.96–4.03 (m, 1 H, $C^\alpha H$), 4.15–4.26 (m, 2 H, N^{PTZ}-CH_2), 4.40 (s, N^{PQ}-CH_3), 4.52 (t, J = 7.1 Hz, 2 H, N^{PQ}-CH_2), 6.80–7.02 (m, 6 H, 4 × PTZ & $N^\alpha H$ & $N^{pr}H$), 7.07–7.18 (m, 4 H, PTZ), 7.24–7.28 (m, 1 H, m5), 7.32–7.43 (m, 4 H, b5), 7.55 (d, J = 5.8 Hz, 1 H, m6′), 7.58–7.74 (m, 6 H, 4 × b6 & m5′ & $N^\epsilon H$), 7.85 (d J = 5.6 Hz, 1 H, m6), 7.97–8.10 (m, 4 H, b4), 8.22–8.36 (m, 4 H, 3,3′,5,5′-PQ), 8.43–8.54 (m, 4 H, b3), 8.80–8.88 (m, 3 H, m3 & 2′6′-PQ), and 8.95 ppm (d, J = 7.1 Hz, 2 H, 2,6-PQ).

General Methods. Uncorrected melting points were obtained with a Fisher-Johns apparatus. UV–vis spectra were recorded on a Hewlett-Packard 8452A photodiode-array spectrophotometer. Infrared spectra were recorded on a Nicolet DX20 Fourier-transform IR spectrophotometer. Mass spectra were recorded with a VG SEQ70 hybrid MS/MS spectrometer. ^1H NMR spectra were recorded at 200 MHz on a Bruker AC 200 spectrometer, or when so noted at 400 MHz on a Varian XL 400. Cation-exchange HPLC was performed with an Aquapore CX-300 column (1.0 cm × 10 cm) of poly(DL-Asp)-silica (Brownlee) with a gradient of 0–400 mM KBr in 2:3 (v/v) CH_3CN/0.6 mM phosphate buffer (pH 7.2). Thin-layer chromatograms were performed on Bakerflex silica gel plates.

Electrochemistry. Tetra(1-butyl)ammonium hexafluorophosphate (Bu_4NPF_6, Fluka) was twice recrystallized from ethanol and vacuum dried for 10 h. UV-grade CH_3CN (Burdick and Jackson) was used as received. Cyclic voltammograms were recorded in 0.1 M Bu_4NPF_6/CH_3CN solutions with a Princeton Applied Research 173 potentiostat/175 universal programmer, a Soltec VP6414S chart recorder, a silver/silver nitrate or SSCE reference electrode, a platinum-wire auxiliary electrode, and a BAS MF-2013 platinum-disk working electrode (0.31 cm^2 electrode area). All half-wave potentials are reported vs SSCE at a scan rate of 200 mV/s.

Photophysical Measurements. Luminescence spectra were obtained with a SPEX Fluorolog 212 photon-counting spectrofluorimeter with 460-nm excitation and 2-mm slit width and are corrected for the instrument response by the procedure supplied by the manufacturer. Emission quantum yields, Φ_{em}, were measured in optically dilute CH_3CN solutions (A_{460} = 0.09–0.13; ~1–5 × 10^{-5} M) relative to $[Ru^{II}(bpy)_3](PF_6)_2$ for which Φ_{em} = 0.0615 in CH_3CN at 295 K.[13] The quantum yields were calculated as reported previously.[14] Emission spectral fitting was conducted according to protocols described previously[15] with the use of GOODFIT, a least-squares fitting program based on a Simplex algorithm and written by J. P. Claude.

Temperature-dependent emission spectra were collected over the range 88–296 K in freeze–pump–thaw degassed 4:1 (v/v) ethanol/methanol with the SPEX Fluorolog 212 spectrofluorimeter. For these measurements, the sample temperature was controlled by use of an Oxford liquid-nitrogen cryostat. The sample was allowed to equilibrate for at least 30 min at each temperature setting prior to conducting the emission measurement.

Absolute quantum yields for decomposition, Φ_P, were measured as described previously[16] at 295 K in a freeze–pump–thaw degassed (four cycles), stirred 0.2 M [n-Bu_4N]Cl/CH_3CN solution. A collimated 75-W Xe lamp was used as the irradiation source. A monochromator was used to isolate the desired 452-nm excitation line, and the intensity of irradiance was measured by use of Reinecke salt, $(NH_4[Cr(NH_3)_2(SCN)_4]\cdot H_2O)$, as a chemical actinometer. Over the course of a 12-h irradiation, the sample was converted to nonemissive products, and the resulting decrease in the emission intensity was monitored with the spectrofluorimeter.

Emission lifetimes were measured with a PRA LN1000/LN 102 nitrogen laser/dye laser combination operated at 460 nm for sample excitation. Emission was monitored at 90° to the excitation with a PRA B204-3 monochromator and a cooled 10-stage Hammamatsu R928 PMT coupled to either a LeCroy 9400 digital oscilloscope or a LeCroy 6880/6010 transient digitizer interfaced to an IBM PC. Samples dissolved in UV-grade CH_3CN (Burdick and Jackson) had an absorbance of ~0.1 at 460 nm (~1 × 10^{-5} M) in a 1-cm quartz cuvette and were bubble-deoxygenated with high-purity argon for at least 10 min. This instrumentation as well as procedures used for treatment of data have been described previously.[14]

Nanosecond transient absorption spectra and kinetics were also collected by means of previously described methods and instrumentation.[14,17,18] The third harmonic (354.7 nm) of a Quanta Ray DCR-2A Nd:YAG laser was used to pump a Quanta Ray PDL-2 dye laser to produce 420-nm, 4-ns excitation pulses with energy of <5 mJ/pulse, which was used to excite the samples. In some cases the second harmonic (532 nm) was used for sample excitation. The excitation beam was coincident at the sample and colinear with the monitoring beam provided by an Applied Photophysics laser kinetic spectrometer, which utilized a 300-W pulsed Xe arc lamp probe source, an $f/3.4$ grating monochromator, and a five-stage PMT. The resulting output was collected with the use of the LeCroy 6880/6010 transient digitizer/IBM PC. Electronic control and synchronization of the laser, probe, and transient digitizer were provided by electronics of our own design. Appropriate Oriel or Corning cutoff filters were used to exclude high-energy probe light, which limited direct irradiation of PTZ by the probe light. UV-grade CH_3CN (Burdick and Jackson) solutions with absorbances of 0.09–0.13 (~1.5 × 10^{-5} M) were bubble-deoxygenated with high-purity argon for at least 10 min. For full-spectrum transient absorption measurements, a sample (35–50 mL) was freeze–pump–thaw degassed to ~10^{-6} Torr in a "tipsy" cell of our own design, which was then sealed. Use of this cell provided a renewable supply of unirradiated sample during the laser experiment, in which small portions (~1.5–2 mL) of solution were transferred to the 1-cm square glass cuvette of the cell, irradiated with a limited number of laser shots, and then tipped into a waste-holding compartment of the cell; the cuvette was then filled with fresh solution from the reservoir compartment of the cell.

Global kinetic analysis of nanosecond transient absorption spectra was performed by using the analysis protocol of Maeder and Zuberbühler.[19] This type of treatment of large, multivariate data sets includes both kinetic[20] and equilibrium studies[21] and is becoming increasingly prevalent since it provides spectra of the components as well as the fitted rate/equilibrium constants. The program SPECFIT[19] was modified[22] to enable kinetic analysis. The treatment uses factor analysis of the data (ΔA, λ, t) to obtain a reduced data set. A Marquardt nonlinear least-squares fitting algorithm provides a simultaneous fit to the reduced data at all wavelengths according to a chosen reaction scheme. In our case, a biexponential function provided an excellent fit to the scheme A → B → C at every wavelength. The spectral components of the transient spectrum in their order of appearance were extracted, and the time-evolution of the transient spectrum was reproduced by the analysis. This procedure provided a very high quality fit of the nanosecond transient data, with error in the rate constants of ±0.3–1.1%.

Picosecond transient absorption spectra were obtained with the equipment of Dr. E. F. Hilinski of Florida State University. This instrument has been described in detail.[23,24] For the transient absorption

(12) Smith, N. L. *J. Org. Chem.* **1950**, *15*, 1125–1130.
(13) Caspar, J. V.; Meyer, T. J. *J. Am. Chem. Soc.* **1989**, *111*, 7448.
(14) Chen, P.; Duesing, R.; Graff, D. K.; Meyer, T. J. *J. Phys. Chem.* **1991**, *95*, 5850.
(15) (a) Caspar, J. V.; Meyer, T. J. *Inorg. Chem.* **1983**, *22*, 2444. (b) Caspar, J. V.; Meyer, T. J. *J. Am. Chem. Soc.* **1983**, *105*, 5583. (c) Kober, E. M.; Caspar, J. V.; Lumpkin, R. S.; Meyer, T. J. *J. Phys. Chem.* **1986**, *90*, 3722.
(16) (a) Durham, B.; Caspar, J. V.; Nagle, J. K.; Meyer, T. J. *J. Am. Chem. Soc.* **1982**, *104*, 4803. (b) Strouse, G. F.; Anderson, P. A.; Schoonover, J. R.; Meyer, T. J.; Keene, F. R. *Inorg. Chem.* **1992**, *31*, 3004. (c) We are indebted to G. F. Strouse for this measurement.
(17) (a) Duesing, R.; Tapolsky, G.; Meyer, T. J. *J. Am. Chem. Soc.* **1990**, *112*, 5378. (b) Danielson, E., in preparation.
(18) Younathan, J.; Jones, W. E.; Meyer, T. J. *J. Phys. Chem.* **1991**, *95*, 488.
(19) Maeder, M.; Zuberbühler, A. D. *Anal. Chem.* **1990**, *62*, 2220.
(20) (a) Knutson, J. R.; Beecham, J. M.; Brand, L. *Anal. Instrum.* **1985**, *14*, 379. (b) Cruse, R. W.; Kaderli, S.; Karlin, K. D.; Zuberbühler, A. D. *J. Am. Chem. Soc.* **1988**, *110*, 6882. (c) Sun, Y.-P.; Fox, M. A.; Johnston, K. P. *J. Am. Chem. Soc.* **1992**, *114*, 1187.
(21) (a) Ozeki, T.; Kihara, H.; Ikeda, S. *Anal. Chem.* **1988**, *60*, 2055. (b) Gampp, H.; Maeder, M.; Meyer, C. J.; Zuberbühler, A. D. *Talanta* **1986**, *33*, 943.
(22) The program SPECFIT, described by Maeder,[19] was modified to perform kinetic analysis by Dr. R. A. Binstead, and we acknowledge Dr. Binstead for his assistance with this analysis.
(23) Schmidt, J. A.; Hilinski, E. F. *Rev. Sci. Inst.* **1989**, *60*, 2902.
(24) We thank Professor E. F. Hilinski of Florida State University for kindly granting us the use of the picosecond transient absorption spectrometer, and we thank K. L. Tate for his assistance in operating the spectrometer.

Table I. Photophysical Data in CH_3CN at 295 K

	compound	λ_{max},[a] nm	Φ_{em}[b]	τ_{em},[c] ns	τ_{rs},[d] ns
1	[PTZpn-Lys($Ru^{II}b_2m$)$^{2+}$-NH-prPQ^{2+}]	645	0.004	18	108
3	[$Ru^{II}b_2m$-NHCH$_3$]$^{2+}$	645	0.087	1380	na
4	[Boc-Lys($Ru^{II}b_2m$)$^{2+}$-OH]	645	0.077	1450	na
5	[($Ru^{II}b_2m$)$^{2+}$-NH-prPQ^{2+}]	645	0.003	<4	<4
6	[($Ru^{II}b_2m$)$^{2+}$-NH-prPTZ]	645	0.005	<4	33
7	[($Ru^{II}b_2m$)$^{2+}$-Ala-Lys(PTZpn)-Ala-OH]	645	0.007	<4	39
8	[PTZpn-Lys($Ru^{II}b_2m$)$^{2+}$-OCH$_3$]	645	0.003	14	23
9	[Boc-Lys($Ru^{II}b_2m$)$^{2+}$-NH-prPQ^{2+}]	645	0.003	40	<1
	[Ru^{II}(bpy)$_3$]$^{2+}$	626	0.062[11]	920[13b]	na

[a] Emission band maximum in nm (±2). [b] Emission quantum yield (±10%). [c] Lifetime (±2–4 ns) obtained by analyzing emission decay curves at the emission maxima following laser excitation at 460 nm. [d] Redox-separated state lifetime (±2–4 ns) obtained by analyzing transient absorption decay curves at 510 and 610 nm following excitation with 420-nm, 4-ns laser pulses. All spectroscopic experiments were conducted in optically dilute solutions ~1–5 × 10^{-5} M.

Table II. $E_{1/2}$ Values in CH_3CN[a]

	compound	PTZpn +/0	[Rub_2m]$^{2+}$ 3+/2+	[Rub_2m]$^{2+}$ 2+/1+	[Rub_2m]$^{2+}$ 1+/0	prPQ^{2+} 2+/1+
1	[PTZpn-Lys($Ru^{II}b_2m$)$^{2+}$-NH-prPQ^{2+}][b]	0.75	1.32	−1.33	−1.51	−0.42
3	[$Ru^{II}b_2m$-NHCH$_3$]$^{2+}$		1.27	−1.28	−1.51	
4	[Boc-Lys($Ru^{II}b_2m$)$^{2+}$-OH]		1.27	−1.31	−1.47	
5	[($Ru^{II}b_2m$)$^{2+}$-NH-prPQ^{2+}][c]		1.29	−1.28	−1.51	−0.42
6	[($Ru^{II}b_2m$)$^{2+}$-NH-prPTZ]	0.75	1.33	−1.22	−1.46	
7	[($Ru^{II}b_2m$)$^{2+}$-Ala-Lys(PTZpn)-Ala-OH]	0.71	1.28	−1.18	−1.44	
8	[PTZpn-Lys($Ru^{II}b_2m$)$^{2+}$-OCH$_3$]	0.76	1.32	−1.33	−1.55	
10	[PTZpn-NH-prPQ^{2+}]	0.76				−0.39
	[Ru^{II}(bpy)$_3$]$^{2+}$ (ref 13b)		1.29	−1.33	−1.52	

[a] $E_{1/2}$ value (±0.02 V) obtained in 0.1 M Bu_4NPF_6/CH_3CN solutions by taking an average of anodic and cathodic peak potentials in cyclic voltammograms acquired with Pt-disc working, Pt-wire auxiliary, and saturated sodium chloride calomel (SSCE) reference electrodes at a scan rate of 200 mV/s. [b] Redox potentials for **1** were estimated from model compounds. [c] Potentials for 2+/1+ and 1+/0 couples are estimated because reduction of **5** beyond −0.6 V vs SSCE led to a rapid catalytic decomposition of the sample.

measurements performed here, the third harmonic (355 nm) of the amplified 1064-nm fundamental of an actively-passively mode-locked Nd:YAG laser was used to pump a Raman shift cell containing CH_4 (100 PSI). Colored glass filters (Corning 3-73 and 5-57) were used to isolate the second Stokes band of CH_4 (447 nm). The 25-ps, 447-nm pulses were used for sample excitation at energies of 0.2–0.3 mJ/pulse. The absorbance change induced in the sample at a selected time after excitation was probed by means of a 25-ps white-light continuum pulse, which was generated when a portion of the 1064-nm laser fundamental was focused into a 20-cm cell containing a 1:1 mixture of H_2O and D_2O. This interrogation pulse was delayed in time with respect to the excitation pulse by means of an adjustable optical delay line. The continuum pulses were split into two equal parts and transmitted through the sample cell and a reference cell and were then focused at the slit of a 0.32-m spectrograph (Model HR-320, Instruments SA) whose output was imaged onto an EG&G Princeton Applied Research (PAR) two-dimensional silicon intensified target (SIT) detector (Model 1254E) coupled to an EG&G PAR multichannel detector controller (Model 1216) that was interfaced with an IBM PC. Difference absorption spectra covering the wavelength range from 400–800 nm were recorded as Δ absorbance vs λ from two spectral windows at times ranging from −50 ps to 20 ns after excitation of the sample. For these experiments, the configuration of the delay line was modified to permit examination of delay times as long as 40 ns following excitation. A mask was used at the face of the SIT detector to minimize the amount of 447-nm excitation reaching the detector and is responsible for the "notch" in the picosecond data in the 447-nm region. Each difference absorption spectrum is the average of the result of ~400 excitation laser shots. The details of acquisition and treatment of the transient absorption data have been described.[23]

For the picosecond experiment, the sample was flowed through a 5-mm quartz cell with a syringe and a mechanical syringe driver. The samples were bubbled with Ar or N_2 immediately prior to the experiment and maintained under a N_2 atmosphere during the experiment. The samples had an absorbance of ~0.1 at 447 nm (~5 × 10^{-5} M) and were monitored by UV–visible absorption spectroscopy to assure that the samples were not decomposed by laser irradiation.

Transient Raman spectra were measured[25] by using the third harmonic (354.7 nm) of the Quanta-Ray DCR-2A pulsed Nd:YAG laser to create the excited state and as a source for the Raman scattering. The sample was degassed by several cycles of freeze–pump–thawing and sealed in an NMR tube. The scattered radiation was collected in a 135° backscattering geometry into a SPEX 1877 Triplemate spectrometer equipped with an 1800 grooves/mm grating. The signal was examined by a Princeton Instruments IRY-700G optical multichannel analyzer operating in the gated mode with a ST-110 OSMA detector controller. Timing was controlled by a Princeton Instruments FG-100 pulse generator. The final spectrum was the result of a total integration time of 16 min. Laser power was 3–5 mJ/pulse. Data collection and storage were controlled by an IBM AT using Princeton Instruments SMA software package.

Results

Model Chromophores: ($Ru^{II}b_2m$)$^{2+}$-NHCH$_3$, 3, and Boc-Lys($Ru^{II}b_2m$)$^{2+}$-OH, 4. Monocarboxylic acid derivatives of the chromophore [Ru^{II}(bpy)$_3$]$^{2+}$ (bpy or b = 2,2′-bipyridine) have been prepared previously.[26,27] A practical synthesis of the bipyridine monocarboxylic acid ligand **2** (4′-methyl-2,2′-bipyridine-4-carboxylic acid, which we abbreviate m-OH) was developed.[9,28] The preparation, shown below, involved the selenium dioxide oxidation of 4,4′-dimethyl-2,2′-bipyridine (Aldrich) followed by silver oxide oxidation of the resulting monoaldehyde and provided the monoacid **2** directly in a 45% overall yield after purification.

The substitution reaction between m-OH and [$Ru^{II}b_2Cl_2$] gave [$Ru^{II}b_2$m-OH]$^{2+}$ in 96% yield.[9] This complex was converted into the *N*-methyl amide **3**, [$Ru^{II}b_2$m-NHCH$_3$]$^{2+}$, which was used as a model chromophore for these assemblies. The acid [$Ru^{II}b_2$m-OH]$^{2+}$ was activated and used for N^{ϵ}-acylation of Boc-lysine (Boc = *tert*-butoxycarbonyl) to furnish the amide **4**, [Boc-

(25) Strommen, D. P.; Mallick, P. K.; Danzer, G. D.; Lumpkin, R. S.; Kincaid, J. R. *J. Phys. Chem.* **1990**, *94*, 1357.

(26) Telser, J.; Cruickshank, K. A.; Schanze, K. S.; Netzel, T. L. *J. Am. Chem.* **1989**, *111*, 7221.

(27) Nussbaumer, W.; Gruber, H.; Greber, G. F. *Monatsh. Chem.* **1988**, *119*, 1.

(28) (a) The synthesis of m-OH was developed by G. F. Strouse as a 24%-yield preparation first reported in the supplementary material of a previous paper.[28b] The synthesis was later improved[9a] to give a 45% yield. A synthesis reported from another laboratory afforded the monoester m-OCH$_3$ by direct selenium dioxide oxidation of 4,4′-dimethyl-2,2′-bipyridine in 51% yield.[28c] (b) Boyde, S.; Strouse, G. F.; Jones, W. E., Jr.; Meyer, T. J. *J. Am. Chem. Soc.* **1990**, *112*, 7395. (c) Wang, G.; Bergstrom, D. E. *Synth. Lett.* **1992**, *5*, 422.

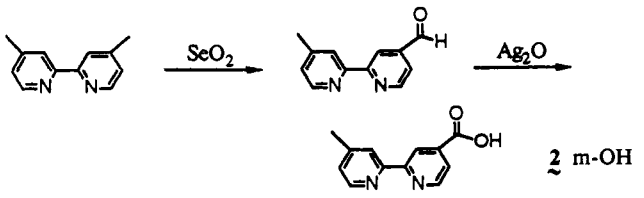

2 m-OH

(4'-Me-2,2'-bpy-4-COOH)

$Lys(Ru^{II}b_2m)^{2+}$-OH], a synthetic amino acid that served as a chromophore module in the preparation of more complex systems.[9]

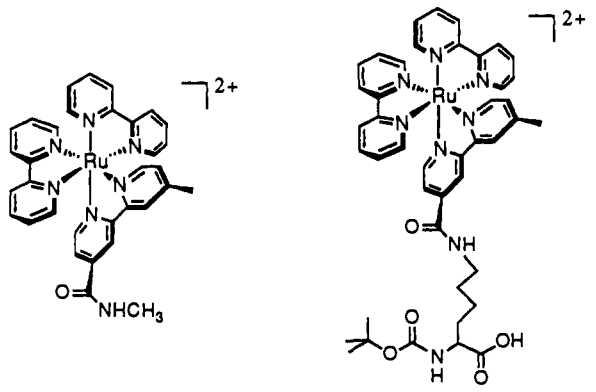

3 $(Ru^{II}b_2m)^{2+}$-$NHCH_3$ 4 Boc-$Lys(Ru^{II}b_2m)^{2+}$-OH

The results obtained from the spectroscopic studies of all the assemblies described here are summarized in Table I, with data for $[Ru^{II}(bpy)_3]^{2+}$ included for comparison. All spectroscopic experiments were conducted in optically dilute solutions with concentrations of $\sim 1-5 \times 10^{-5}$ M unless otherwise noted. Electrochemical data are given in Table II. In **3**, the reduction potential for the $Ru^{III/II}$ couple is $E_{1/2} = 1.27$ V (vs SSCE) and for the first ligand-based reduction, $E_{1/2} = -1.28$ V. For **4**, these potentials are nearly the same: $Ru^{III/II}$, $E_{1/2} = 1.27$ V and $bpy^{0/-}$, $E_{1/2} = -1.31$ V. For **3**, **4**, and the remaining ruthenium complexes studied, the $d\pi(Ru^{II}) \rightarrow \pi^*$(b,m) metal-to-ligand charge-transfer (MLCT) absorption band was observed at 456 nm with $\epsilon \cong 11\,700$ L mol^{-1} cm^{-1}. Emission from $[Ru^{II}b_2m\text{-}NHCH_3]^{2+}$ occurred with $\lambda_{max} = 645$ nm, a quantum yield of 0.087 ± 0.009, and a lifetime of 1380 ns ($k = 7.25 \times 10^5\ s^{-1}$) in CH_3CN. The absorption and emission spectra for **3** are shown in Figure 1a. The transient absorption spectrum of **3** is characterized by a strong negative absorption at 460 nm due to depopulation (bleaching) of the MLCT ground state and a strong positive signal at 370 nm due to the absorption of the bipyridyl anion radical ($b_2m^{\bullet-}$) and is essentially the same as the transient spectrum observed for the parent $[Ru^{II}(bpy)_3]^{2+}$. The photophysical behavior of **4** is very similar to that of **3**. Emission from **4** occurred with $\lambda_{max} = 645$ nm, a quantum yield of 0.077 ± 0.008, and a lifetime of 1450 ns ($k = 6.9 \times 10^5\ s^{-1}$) in CH_3CN.

The photostability of the model chromophore **3** was examined. The quantum yield for photosubstitution, $\Phi_P = 0.030 \pm 0.003$, was measured at 295 K in 0.2 M Bu_4NCl/CH_3CN with 452-nm excitation.[16] Data from temperature-dependent emission measurements conducted in 4:1 (v/v) ethanol/methanol in the temperature range 88–296 K (Figure 2) show that the emission intensity from **3** decreases very little (less than 1.5 orders of magnitude) with increasing temperature. In Figure 2, the glass-to-fluid transition is responsible for the shape of the curve near 130 K, and only slight temperature dependence is otherwise apparent. For comparison, note that in systems which show significant temperature dependence, the emission intensity may decrease by five to eight orders of magnitude over a similar temperature range.[29]

Time-resolved resonance Raman spectra of **3**, $[Ru^{II}b_2m\text{-}NHCH_3]^{2+}$, and $[Ru^{II}(m\text{-}NHCH_3)_3]^{2+}$ (see structure below) in

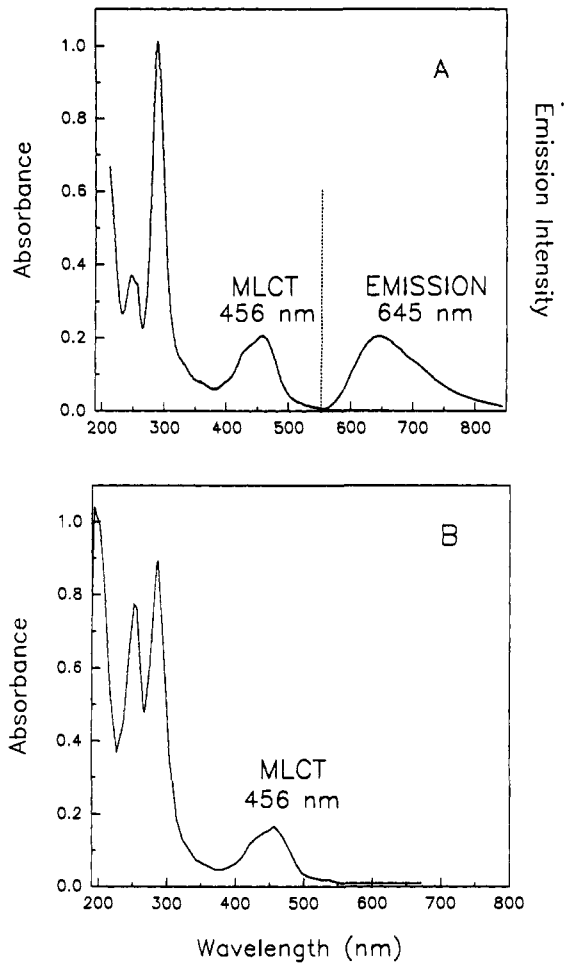

Figure 1. (a) UV–visible absorption spectra (normalized, left axis) and emission spectra (scaled arbitrarily, right axis) in CH_3CN for **3**, $[Ru^{II}b_2m\text{-}NHCH_3]^{2+}$. (b) Normalized UV–visible absorption spectra in CH_3CN for **1**, [PTZpn-$Lys(Ru^{II}b_2m)^{2+}$-NH-$prPQ^{2+}$]. Samples were $\sim 5 \times 10^{-4}$ M with $\epsilon_{456\ nm} = 11\,700$ L mol^{-1} cm^{-1} and were the PF_6^- salts.

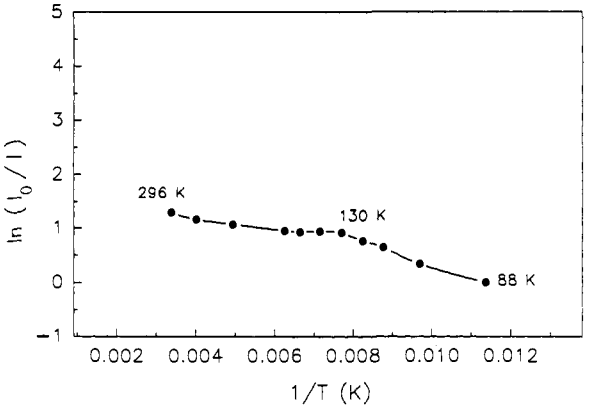

Figure 2. Temperature-dependent emission data for **3**, $[Ru^{II}b_2m\text{-}NHCH_3]^{2+}$, in 4:1 ethanol/methanol. Each data point represents the integrated emission intensity over the range of 500–800 nm at a selected temperature, and the data set is normalized to the integrated emission intensity at 88 K.

CH_3CN are shown in Figure 3. The spectra in Figure 3 were obtained under the same conditions as those previously reported[25] for collection of the transient Raman spectrum of $[Ru^{II}(bpy)_3]^{2+}$, in which 354.7-nm laser pulses were used both to excite the sample and as a source for the Raman scattering. The excited-state Raman spectrum of **3** (Figure 3a) is virtually identical with that of $[Ru^{II}(m\text{-}NHCH_3)_3]^{2+}$ (Figure 3b) and is significantly different from that of $[Ru^{II}(bpy)_3]^{2+}$.[25] These results indicate that the electron in the excited state is localized primarily in the π^* level

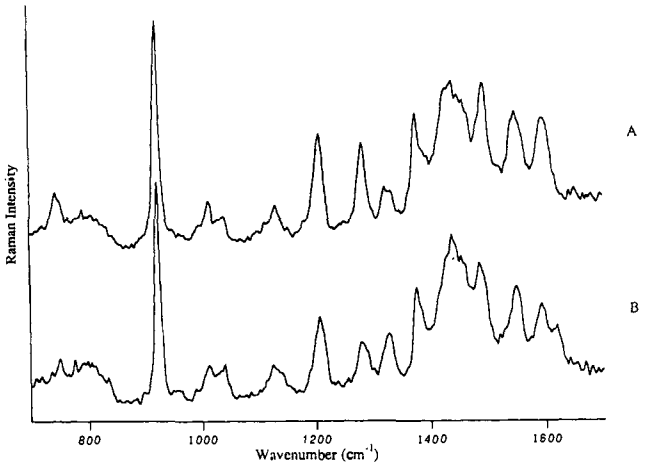

Figure 3. Time-resolved resonance Raman spectra of **3**, $[Ru^{II}b_2m\text{-}NHCH_3]^{2+}$ (A, upper spectrum) and $[Ru^{II}(m\text{-}NHCH_3)_3]^{2+}$ (B, lower spectrum) in CH_3CN. The spectra were measured as described in the Experimental Section and represent a total integration time of 16 min. Excited-state Raman peaks for m-$NHCH_3$ appear at 745, 1012, 1037, 1131, 1209, 1283, 1429, 1441, 1494, and 1552 cm^{-1}. Peaks at 1327 and 1598 cm^{-1} are ground-state bpy (b) peaks. Solvent peaks appear at 923 and 1377 cm^{-1}.

of the amide ligand m-$NHCH_3$ in **3**. Excited-state resonance Raman peaks for **3** appear at 745, 1012, 1037, 1131, 1209, 1283, 1429, 1441, 1494, and 1552 cm^{-1} under these conditions. The peaks seen at 923 and 1377 cm^{-1} are solvent (CH_3CN) peaks. Peaks for $bpy^{\bullet-}$ are not observable, but ground-state bpy peaks are detected in the transient Raman spectrum of **3** at 1327 and 1598 cm^{-1}; the peak at 1494 cm^{-1} may be an overlap of ground-state bpy and excited-state m-$NHCH_3$. No ground-state m-$NHCH_3$ peaks are observed, as determined by comparison with the ground-state resonance Raman spectrum of $[Ru^{II}(m\text{-}NHCH_3)_3]^{2+}$.

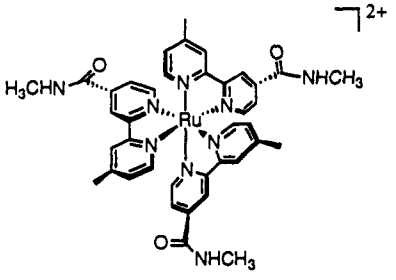

$[Ru^{II}(m\text{-}NHCH_3)_3]^{2+}$

Chromophore–Quencher Dyads: $[(Ru^{II}b_2m)^{2+}\text{-}NH\text{-}prPQ^{2+}]$, 5, and $[(Ru^{II}b_2m)^{2+}\text{-}NH\text{-}prPTZ]$, 6. The initial approach taken in the construction of amide-linked assemblies for studies of photoinduced intramolecular electron transfer was to join an appropriately derivatized quencher to the model chromophore with an amide bond. The oxidative quencher paraquat (PQ^{2+}, $E_{1/2} = -0.42$ V vs SSCE) was attached to the chromophore through a trimethylene spacer. In CH_3CN at 25 °C, the resulting dyad **5**, $[(Ru^{II}b_2m)^{2+}\text{-}NH\text{-}prPQ^{2+}]$, exhibited efficient (97%) quenching of the MLCT luminescence. The quantum yield for emission was reduced to 0.003 ± 0.001 and the emission lifetime of <4 ns was too short to be accurately resolved with our PMT-based detection system. A long-lived component of $\tau \sim 1.3$ μs made a small contribution (<2%) to the emission decay and could be attributed to unquenched MLCT luminescence arising from an impurity. By nanosecond transient absorption spectroscopy, an absorption at 370 nm and a bleach (negative absorption) at 460 nm were both observed to appear promptly and recover to the preexcitation level with $\tau < 4$ ns following excitation with 420-nm, 4-ns pulses. No other transient signals were observed;

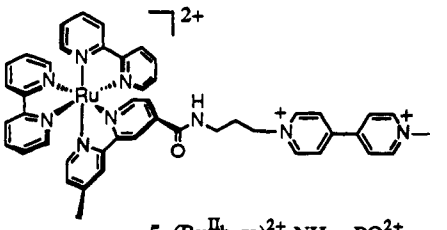

5 $(Ru^{II}b_2m)^{2+}\text{-}NH\text{-}prPQ^{2+}$

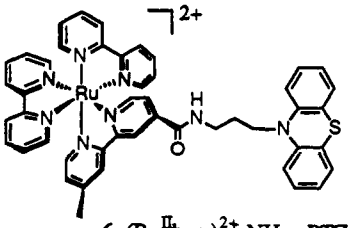

6 $(Ru^{II}b_2m)^{2+}\text{-}NH\text{-}prPTZ$

specifically, no signal arising from reduced paraquat ($PQ^{\bullet+}$), expected in the 610-nm region,[30] was observed. From these observations it can be inferred that the MLCT state is quenched by a rapid forward electron transfer that occurs from the ligand anion radical ($b_2m^{\bullet-}$) to the acceptor (PQ^{2+}) with $k_f > 2.5 \times 10^8$ s^{-1} (Scheme I). This is followed by an even faster back electron transfer, $k_b \gg k_f$, from the reduced acceptor ($PQ^{\bullet+}$) to the Ru^{III} metal center, which returns the system to the ground state. The redox-separated state $[(Ru^{III}b_2m)^{3+}\text{-}NH\text{-}(prPQ^{\bullet+})]$ does not accumulate in sufficient concentration to be observed by transient absorption spectroscopy.

The excited-state energy of 2.15 eV given in Scheme I and the following schemes was estimated from parameters obtained from emission spectral fitting[15] of the room temperature emission spectrum of the model chromophore **3**, $[Ru^{II}b_2m\text{-}NHCH_3]^{2+}$, in CH_3CN.[31]

An aminopropyl derivative of the reductive quencher phenothiazine (PTZpnOH, $E_{1/2} = 0.75$ V) was similarly attached to the chromophore by an amide linkage to form compound **6**, $[(Ru^{II}b_2m)^{2+}\text{-}NH\text{-}prPTZ]$ (shown above). The MLCT luminescence in CH_3CN at 25 °C was also largely quenched with $\Phi_{em} = 0.005 \pm 0.001$ and $\tau_{em} < 4$ ns. Nanosecond transient absorption spectroscopy of $[(Ru^{II}b_2m)^{2+}\text{-}NH\text{-}prPTZ]$ confirmed that elec-

(29) (a) In Hecker, C. R.; Gushurst, A. K. I.; McMillin, D. R. *Inorg. Chem.* **1991**, *30*, 538, it was reported that the lifetime of $Ru(tpy)_3^{2+}$ (tpy is 2,2′:6′,2″-terpyridine) in 4:1 ethanol/methanol was observed to vary six orders of magnitude over a 90° temperature range. It was found in our laboratories[29b] that the relative quantum yield for $Ru(tpy)_3^{2+}$ also varied by six orders of magnitude over a similar temperature range. For other systems, variations in relative emission intensity (which is proportional to the quantum yield) of five to eight orders of magnitude were observed in the range 77–298 K.[29b] For the parent $Ru(bpy)_3^{2+}$, in which the dd states are accessed by thermal population, the relative emission intensity[29c] decreases roughly three times more than emission from $Ru(b_2m\text{-}NHCH_3)^{2+}$ between 140 and 295 K. (b) Thompson, D. W., unpublished results. (c) Wacholtz, W. M.; Auerbach, R. A.; Schmehl, R. H.; Ollino, M.; Cherry, W. R. *J. Phys. Chem.* **1985**, *24*, 1758.

(30) Watanabe, T.; Honda, K. *J. Phys. Chem.* **1982**, *86*, 2617.

(31) (a) Emission spectral fitting[15] of data obtained at 88 K in 4:1 EtOH/MeOH gave values for a two mode fit of $E_{00} = 17\,230$ cm^{-1}, $S_m = 0.94$, $\hbar\omega_m = 1430$, $S_1 = 2.32$, $\hbar\omega_1 = 380$, and $\Delta\nu_{1/2} = 622$ cm^{-1}. In the emission spectral fitting procedure, E_{00} is defined as the difference in energy between the ground and excited states in the $v = 0$ vibrational levels of the acceptor vibrations for the two contributing modes, S_m and S_1 are the electron-vibrational coupling constants (Huang-Rhys factors) for the average medium- and low-frequency acceptor modes, $\hbar\omega_m$ and $\hbar\omega_1$ are the quantum spacing, and $\Delta\nu_{1/2}$ is the full width at half maximum for a single vibronic component. Because of the absence of vibronic structure in the room-temperature spectrum, it was fit by a single, average medium frequency mode ($S_m = 0.88$, $\hbar\omega_m = 1430$ cm^{-1}), 0–0 energy $E_0 = 15690$ cm^{-1}, and full-width-at-half-maximum $\Delta\bar{\nu}_{0,1/2} = 1943$ cm^{-1}. In this procedure, $\Delta\bar{\nu}_{0,1/2}$ is related to the sum of the solvent reorganizational energy (χ_0) and the contribution from low-frequency modes treated classically[15c,31b] (χ_1') by $\chi' = \chi_0 + \chi_1' = (\Delta\bar{\nu}_{0,1/2})^2(16k_BT\ln 2)^{-1} = 1660$ cm^{-1}. With these definitions the free energy content of the excited state above the ground state ($\Delta G°_{es}$) is given by $\Delta G°_{es} = E_0 + \chi' = 2.15$ eV.[31b,c] (b) Hupp, J. T.; Neyhart, G. A.; Meyer, T. J.; Kober, E. M. *J. Phys. Chem.* **1993**, *97*, 10820. (c) Worl, L. A.; Duesing, R.; Chen, P.; Della Ciana, L.; Meyer, T. J. *J. Chem. Soc., Dalton Trans.* **1991**, 849.

Scheme I

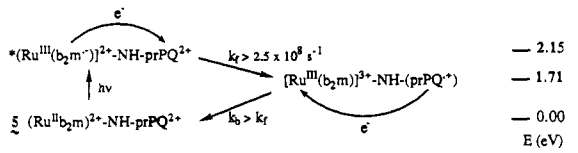

tron transfer from PTZ to Ru^{III} occurred rapidly, as evidenced by recovery of the bleach at 460 nm with $\tau < 4$ ns ($k_f > 2.5 \times 10^8$ s^{-1}). The resulting redox-separated state, [($Ru^{II}b_2m^{\bullet-}$)$^+$-NH-($prPTZ^{\bullet+}$)], was clearly observed with absorptions at 370 nm due to ($b_2m^{\bullet-}$) and 517 nm due to ($prPTZ^{\bullet+}$).[32] This state decays by back electron transfer to the ground state with $\tau = 33$ ns ($k_b = 3 \times 10^7$ s^{-1}) at room temperature in CH_3CN (Scheme II). From the potential differences between the $PTZpn^{+/0}$ and [($Ru^{II}b_2m$—)]$^{2+/+}$ redox couples, it is estimated that the energy of the redox-separated state above the ground state is $\Delta G^\circ \sim 1.97$ eV.

A Chromophore–Quencher Peptide: [($Ru^{II}b_2m$)$^{2+}$-Ala-Lys(PTZ-pn)-Ala-OH], 7. The redox-active tripeptide **7** was successfully prepared[9] by solid-phase peptide synthesis on a Boc-Ala-CH_2-Pam polystyrene resin (Pam is phenylacetamidomethyl) by means of a modified procedure[33] which used BOP [(1-benzotriazoleoxy)tris(dimethylamino)phosphonium hexafluorophosphate)] as the coupling reagent. The coupling (amide-bond forming) steps each proceeded in >98% yield. The peptide was cleaved from the resin cleanly with anhydrous HF. This preparation demonstrated that both the phenothiazine ring system and the ruthenium chromophore are stable to the acidic and basic conditions used for the Boc/benzyl strategy[34] of solid-phase peptide synthesis and are readily incorporated into a peptide chain. In peptide **7** the reductive quencher PTZ is attached to the chromophore by a flexible 12-atom chain containing two *trans* amide bonds.

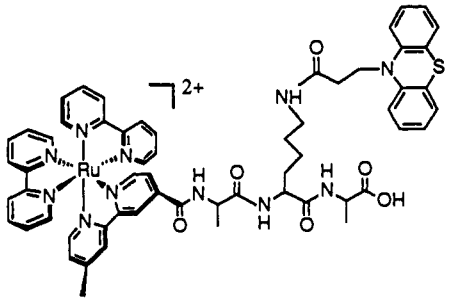

7 ($Ru^{II}b_2m$)$^{2+}$-Ala-Lys(PTZpn)-Ala-OH

In peptide **7**, the reduction potential for the $Ru^{III/II}$ couple is $E_{1/2} = 1.28$ V, and for the $bpy^{0/-}$ couple is $E_{1/2} = -1.18$ V, values very close to those of the model chromophore **3**. The $PTZpn^{+/0}$ couple is at $E_{1/2} = 0.71$ V. The MLCT luminescence from the chromophore of **7** was largely quenched by the attached PTZpn with $\Phi_{em} = 0.007 \pm 0.001$ and $\tau_{em} < 4$ ns. Nanosecond transient absorption spectroscopy of **7** also showed that electron transfer to Ru^{III} occurs very rapidly, as evidenced by recovery of the bleach at 460 nm with $\tau < 4$ ns. The resulting redox-separated state, [($Ru^{II}b_2m^{\bullet-}$)$^+$-Ala-Lys($PTZpn^{\bullet+}$)-Ala-OH], was observed with absorptions at 370 nm due to ($b_2m^{\bullet-}$) and 517 nm due to ($PTZpn^{\bullet+}$). This state decayed with a lifetime of 39 ns ($k_b = 2.6 \times 10^7$ s^{-1}) at room temperature in CH_3CN, in a manner similar to that shown for compound **6** in Scheme II.

Derivatized Amino Acids: The Chromophore–Quencher Dyads [PTZpn-Lys($Ru^{II}b_2m$)$^{2+}$-OMe], 8, and [Boc-Lys($Ru^{II}b_2m$)$^{2+}$-NH-$prPQ^{2+}$], 9. Two new redox-active amino acid derivatives were

Scheme II

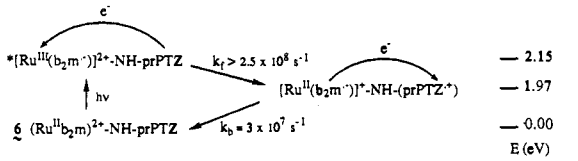

assembled on a lysine scaffold by attaching either an electron donor or an electron acceptor to the lysine-ruthenium chromophore **4**. For assembly of the amino acid derivative **8**, the protective Boc group of [Boc-Lys($Ru^{II}b_2m$)$^{2+}$-OCH_3] was removed with 4 N HCl/dioxane and the freed α-amino group was then acylated with PTZpn-OH with the coupling reagent PyBOP [(1-benzotriazoleoxy)tris(pyrrolidino)phosphonium hexafluorophosphate] and the tertiary base *N*-methylmorpholine in dimethylformamide. For preparation of the amino acid derivative **9**, the amino group of H_2N-$prPQ^{2+}$ was coupled with the free α-carboxy group of **4**, [Boc-Lys($Ru^{II}b_2m$)$^{2+}$-OH], with the use of the same coupling reagents.

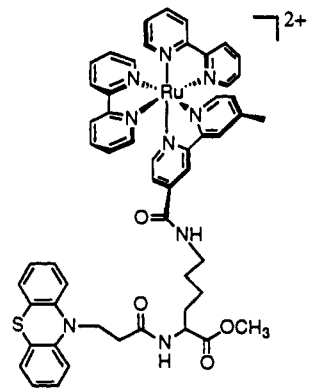

8 PTZpn-Lys($Ru^{II}b_2m$)$^{2+}$-OCH_3

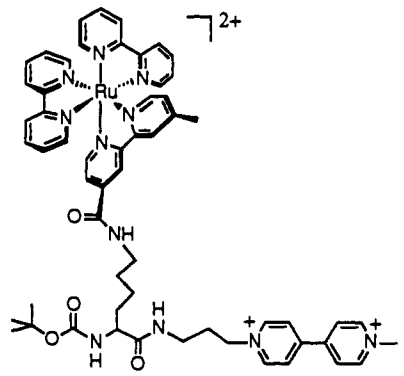

9 Boc-Lys($Ru^{II}b_2m$)$^{2+}$-NH-$prPQ^{2+}$

With the attached electron donor and/or acceptor, the emission from the chromophore was efficiently quenched. For **8**, [PTZpn-Lys($Ru^{II}b_2m$)$^{2+}$-OCH_3], in CH_3CN at 25 °C, $\Phi_{em} = 0.003 \pm 0.001$ and $\tau_{em} = 14 \pm 4$ ns ($k_f = 7.1 \times 10^7$ s^{-1} in Scheme III). Following nanosecond laser-flash photolysis of dyad **8**, the redox-separated state [($PTZpn^{\bullet+}$)-Lys($Ru^{II}b_2m^{\bullet-}$)$^+$-OCH_3] was observed and exhibited a lifetime of $\tau = 23$ ns ($k_b = 4.3 \times 10^7$ s^{-1} in Scheme III).

For dyad **9**, [Boc-Lys($Ru^{II}b_2m$)$^{2+}$-NH-$prPQ^{2+}$], $\Phi_{em} = 0.003 \pm 0.001$ and $\tau_{em} = 40 \pm 4$ ns ($k_f = 2.5 \times 10^7$ s^{-1} in Scheme IV). There was no evidence for the appearance of $prPQ^{\bullet+}$ in transient absorption difference spectra of **9**, even though the MLCT emission was efficiently quenched. Picosecond transient absorption spectroscopy following excitation of **9** in CH_3CN with 447-nm, 25-ps pulses detected the bleaching of the MLCT

(32) Alkaitis, S. A.; Beck, G.; Grätzel, M. *J. Am. Chem. Soc.* **1975**, *97*, 5723.
(33) Fournier, A.; Wang, C. T.; Felix, A. M. *Int. J. Peptide Protein Res.* **1988**, *31*, 86.
(34) Erickson, B. W.; Merrifield, R. B. *Proteins* **1976**, *2*, 255.

Scheme III

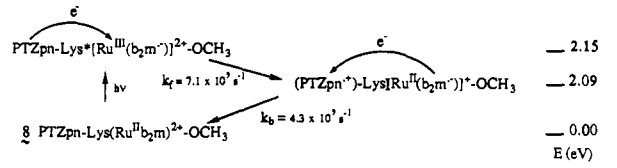

Scheme IV

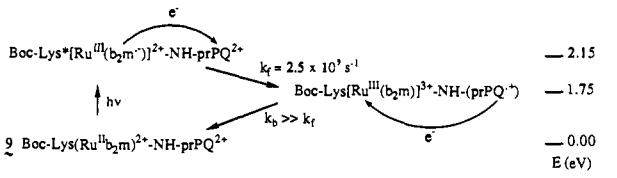

absorption band in the 440–460-nm region. Recovery of the bleach occurred with approximately the same rate as that observed by nanosecond absorption spectroscopy, but $PQ^{\bullet+}$ was not observed even at times as short as 50 ps after excitation. From these observations it can be inferred that the MLCT state is quenched by a forward electron transfer that occurs from the ligand anion radical ($b_2m^{\bullet-}$) to the acceptor (PQ^{2+}) with $k_f = 2.5 \times 10^7\ s^{-1}$ (Scheme IV). This is followed by a fast back electron transfer, $k_b \gg k_f$ in Scheme IV, from the reduced acceptor ($PQ^{\bullet+}$) to the Ru^{III} metal center, which returns the system to the ground state. The redox-separated state [$(Ru^{III}b_2m)^{3+}$-NH-($prPQ^{\bullet+}$)] does not accumulate in sufficient concentration to be observed by transient absorption spectroscopy, similar to the observation for dyad **5** in Scheme I.

Derivatized Amino Acids: The Chromophore–Quencher Triad [PTZpn-Lys($Ru^{II}b_2m$)$^{2+}$-NH-$prPQ^{2+}$], 1. The lysine-based triad **1** (shown above) combines the chromophore with both an electron donor and an acceptor. The preparation of **1** was accomplished[9c] by removing the Boc group of **9**, Boc-Lys($Ru^{II}b_2m$)$^{2+}$-NH-$prPQ^{2+}$, with 4 N HCl/dioxane and coupling the free α-amino group to PTZpn-OH with PyBOP and NMM in DMF. Triad **1** was obtained in 56% yield after purification by cation-exchange HPLC.

The UV–visible absorption spectrum of **1** in acetonitrile is shown in Figure 1b. Comparison with the UV–visible spectrum of the model chromophore **3** (Figure 1a) shows that there is an additional strong absorption at 258 nm in **1** arising from $\pi \rightarrow \pi^*$ absorptions of PTZpn and $prPQ^{2+}$, but the MLCT absorption at 458 nm is not perturbed. A weak residual luminescence observed from **1** in CH_3CN at 295 K has $\tau_{em} = 18 \pm 4$ ns ($k = 5.6 \times 10^7\ s^{-1}$).

Picosecond time-resolved absorption spectra obtained at several time delays after 447-nm, 25-ps pulsed excitation of **1** in argon-bubbled CH_3CN are shown in Figure 4. Delta absorbance versus wavelength (ΔA vs λ) plots were obtained for the wavelength range 400–780 nm. The spectra were corrected for emission. At 50 ps after laser excitation (Figure 4a), a bleach in the 420–480-nm region due to the loss of the ground state, $d\pi(Ru^{II}) \rightarrow \pi^*$(b,m) absorption was observed. The sharp notch in the center of the bleach in Figure 4 results from the use of a physical mask, which blocks the 447-nm laser excitation from the detector. By 650 ps after excitation, the bleach began to recover and new, positive absorptions in the 500–700-nm region appeared. The bleach continued to recover while the new absorptions increased in intensity; by 10 ns (Figure 4b) significant spectral evolution had occurred. The spectrum continued to evolve through the longest time after excitation that could be probed, 40 ns. At 40 ns (Figure 4c), the bleach had recovered to the preexcitation baseline, and maxima at ~510 and 605 nm became apparent. The band at 510 nm is due to $PTZpn^{\bullet+}$,[32] while the band at 605 nm is due to $prPQ^{\bullet+}$.[30] The difference spectrum corresponds to a superposition of the spectra of $PTZpn^{\bullet+}$ and $prPQ^{\bullet+}$, consistent with the formation of the redox-separated state [(PTZpn$^{\bullet+}$)-Lys($Ru^{II}b_2m$)$^{2+}$-NH-($prPQ^{\bullet+}$)] (eq 1, above). The time-profile for the rise of the redox-separated state absorptions and the recovery of the bleach are shown in Figure 5. The redox-separated state, as monitored at 520 (filled circles) and 620 nm (open circles), appeared with a rate of $k = 7.25 \times 10^7\ s^{-1}$ ($\tau = 13.8$ ns). The recovery of the bleach (monitored at 430 nm, open diamonds) occurred with essentially the same rate constant. For this analysis, wavelengths offset from the peak maxima were used so that more accurate ΔA values could be obtained.

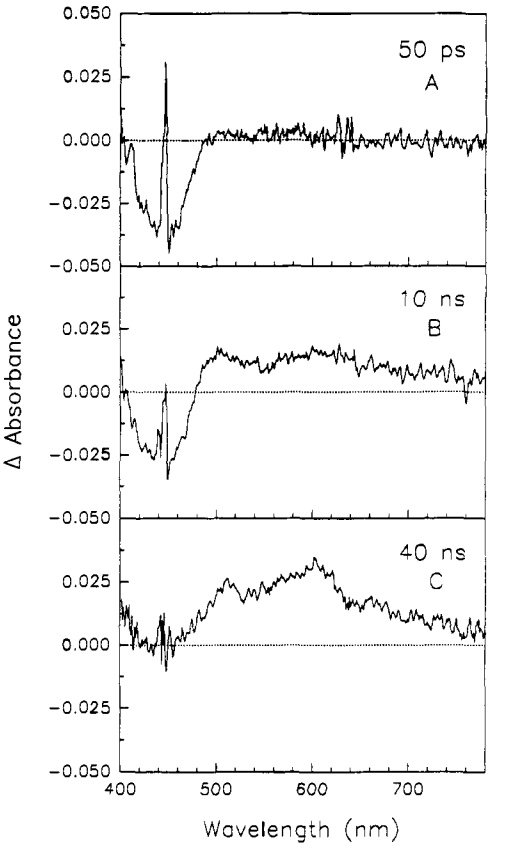

Figure 4. Picosecond transient absorption spectra recorded after excitation of a 5×10^{-5} M solution of **1**, [PTZpn-Lys($Ru^{II}b_2m$)$^{2+}$-NH-$prPQ^{2+}$], in CH_3CN with a 447-nm, 25-ps laser pulse. A mask was used at the face of the SIT detector to minimize the amount of 447-nm excitation reaching the detector and is responsible for the "notch" in the picosecond data in the 447-nm region. Each difference absorption spectrum is the average of the result of ~400 excitation laser shots. The average excitation pulse energy was 0.186 mJ/pulse. The energy dependence of the signal intensity was linear in this energy regime.

Nanosecond transient absorption difference spectra of **1** in freeze–pump–thaw degassed CH_3CN acquired at various times after excitation with a 420-nm, 4-ns laser pulse (≤5.2 mJ/pulse) are shown in Figure 6. The spectra were corrected for emission. The top panel of Figure 6 shows the growth of the spectrum to its maximum intensity and is similar to the picosecond absorption spectra shown in Figure 4, except that a slightly different wavelength range of 320–700 nm was examined in the nanosecond experiment. The lower panel of Figure 6 shows the subsequent decay of the spectrum. These spectra were acquired as ΔA vs time decay traces at a series of selected wavelengths. The ΔA vs λ spectra shown in Figure 6 were obtained by taking cross sections of the set of decay traces at selected times. At 10 ns after the excitation pulse (Figure 6, top panel), increased absorbance at 370 nm due to the bipyridyl anion radical was observed, bleaching due to the loss of the ground-state, $d\pi(Ru^{II}) \rightarrow \pi^*$(b,m) absorption is evident at 440–460 nm, and developing absorptions appear in the 500–700-nm region. This is very similar to the picosecond spectrum shown in Figure 4b at 10 ns. At later times, 15 and 35 ns, the 370-nm absorption ($b_2m^{\bullet-}$) shifted to 390 nm ($prPQ^{\bullet+}$),[30] the bleaching disappeared, and absorptions in

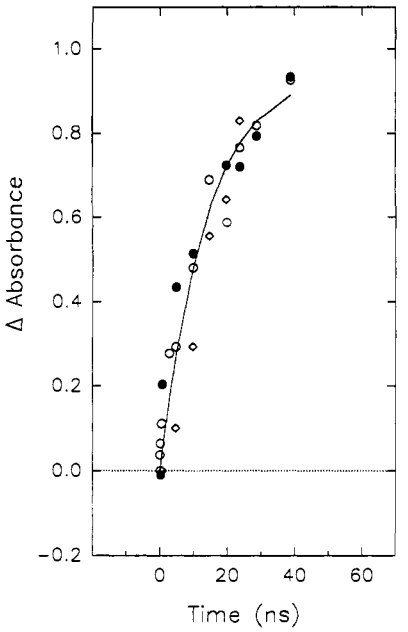

Figure 5. Rise kinetics for the transient absorption spectra depicted in Figure 4. The change in signal intensity with time was monitored at 430 nm (open diamonds, recovery of the bleach) 520 nm (filled circles, $PTZpn^{\bullet+}$), and 620 nm (open circles, $prPQ^{\bullet+}$). The maximum absorbance change was 0.03. The solid line represents a fitted curve for the decay; the rise time is 13.8 ns ($k = 7.25 \times 10^7$ s^{-1}).

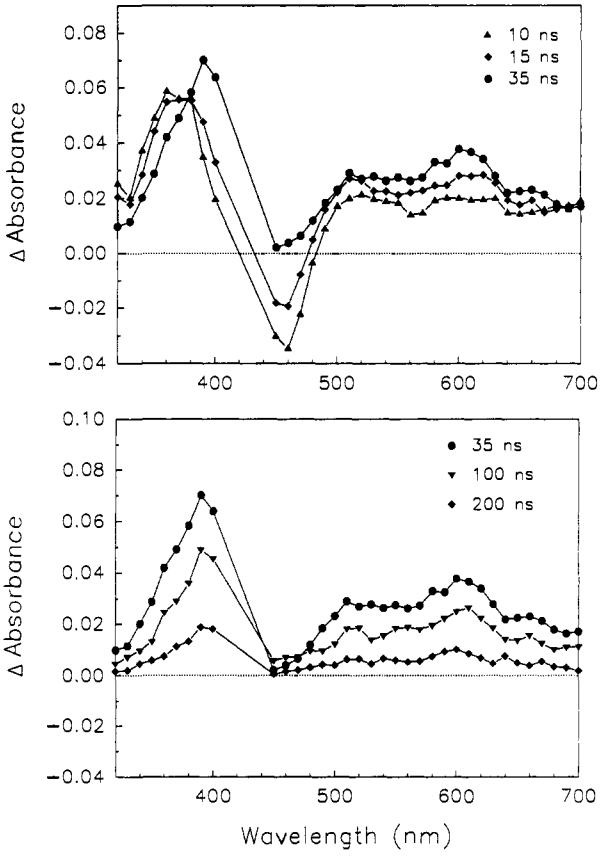

Figure 6. Nanosecond transient absorption difference spectra obtained following 420-nm, 4-ns pulsed (≤5.2 mJ/pulse) excitation of a CH_3CN solution ~1×10^{-5} M in **1**, [PTZpn-Lys($Ru^{II}b_2m$)$^{2+}$-NH-$prPQ^{2+}$] at 25 °C. Top panel: rise of transient spectrum; bottom panel: decay of transient spectrum.

the visible region increased in intensity with maxima at 510 ($PTZpn^{\bullet+}$)[32] and 605 nm ($prPQ^{\bullet+}$).[30] The bleach recovered with $\tau \sim 14$ ns ($k_1 = 7.1 \times 10^7$ s^{-1} in Scheme V), which correlates well with rise times for the 510- and 605-nm bands and is consistent

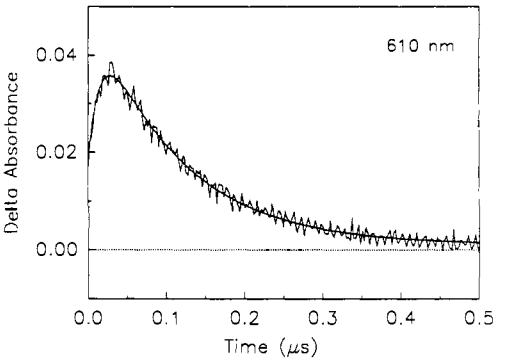

Figure 7. Fitted decay trace for data obtained at 610 nm. The smooth curve is the computer-generated fit to a biexponential function with rate constants of $k = (6.82 \pm 0.07) \times 10^7$ s^{-1} ($\tau = 14.7 \pm 1$ ns) and $(9.26 \pm 0.03) \times 10^6$ s^{-1} ($\tau = 108 \pm 1$ ns).

with the picosecond observations. By 35 ns after the excitation pulse, the difference spectrum corresponding to the redox-separated state, [($PTZpn^{\bullet+}$)-Lys($Ru^{II}b_2m$)$^{2+}$-NH-($prPQ^{\bullet+}$)], reached its maximum intensity, after which the spectrum decayed monoexponentially to the baseline with a lifetime of 108 ± 3 ns ($k_7 = 9.26 \pm 0.2 \times 10^6$ s^{-1}). The bottom panel of Figure 6 shows the decay of the spectrum, while Figure 7 illustrates the kinetic decay observed at 610 nm and a biexponential fit to these data, with a 14-ns rise and a 108-ns decay. The full nanosecond transient absorption spectrum was subjected to global kinetic analysis as described in the Experimental Section. The entire data set of transient decays at 37 wavelengths in the range 320–700 nm was rigorously fit by a biexponential function according to the reaction scheme A → B → C, with the first rate constant of 7.1×10^7 s^{-1} (14 ns) and the second rate constant of 9.26×10^6 s^{-1} (108 ns). The latter corresponds to the redox-separated state lifetime and is different from that previously reported[1] because the application of global kinetic analysis, only recently available to us, provided a significantly more accurate analysis of all the available data.

Measured at its maximum appearance, the redox-separated state was formed with a quantum yield of $\Phi_{rs} = 0.34 \pm 0.03$. This value was measured relative to the known efficiency of formation of $PQ^{\bullet+}$ following oxidative quenching of $[Ru^{II}(bpy)_3]^{2+}$ by paraquat (PQ^{2+}) in CH_3CN after 420-nm excitation.[35]

In order to establish that direct electron transfer between PTZpn and $prPQ^{2+}$ did not play a role in the formation of the redox-separated state following excitation of the triad **1**, the dyad **10**, [PTZpn-NH-$prPQ^{2+}$], was prepared. Dyad **10** is a blue-black solid but in dilute CH_3CN solution has no ground-state UV–visible absorption above 375 nm and does not absorb light at the laser excitation wavelengths (≥420 nm). In contrast, a solution of 10-methylphenothiazine (CH_3-PTZ) and paraquat (PQ^{2+}), ≥0.25 M in each in CH_3CN, showed a charge-transfer absorption at 500 nm for the resulting bimolecular donor–acceptor complex. In addition, the visible region of the absorption spectrum of **1** is identical with that of the model chromophore **3** and does not appear to be perturbed by any additional absorptions from a PTZ/PQ^{2+} charge-transfer complex. These results provide support for the existence of conformations of both **1** and **10** in which the PTZpn and $prPQ^{2+}$ groups do not attain the geometry necessary to form a direct charge-transfer complex in solution.

Energy Conversion Based on the Redox-Separated State. It is possible to convert the stored energy of the redox-separated state into chemical redox energy.[36] This experiment demonstrates a mechanism for interfacing the energy harvesting peptide with an external system and thus shuttling the stored energy further away from the original chromophore. The triad **1** was irradiated with 532-nm excitation in freeze–pump–thaw–degassed CH_3CN in the presence of both 4 mM tetramethylbenzidine (TMBD) and

(35) Olmsted, J., III; Meyer, T. J. *J. Phys. Chem.* **1987**, *91*, 1649.

Scheme V

$$k_{obs} = k_1 + k_4 + k_r + k_{nr} = 7.1 \times 10^7\ s^{-1}$$

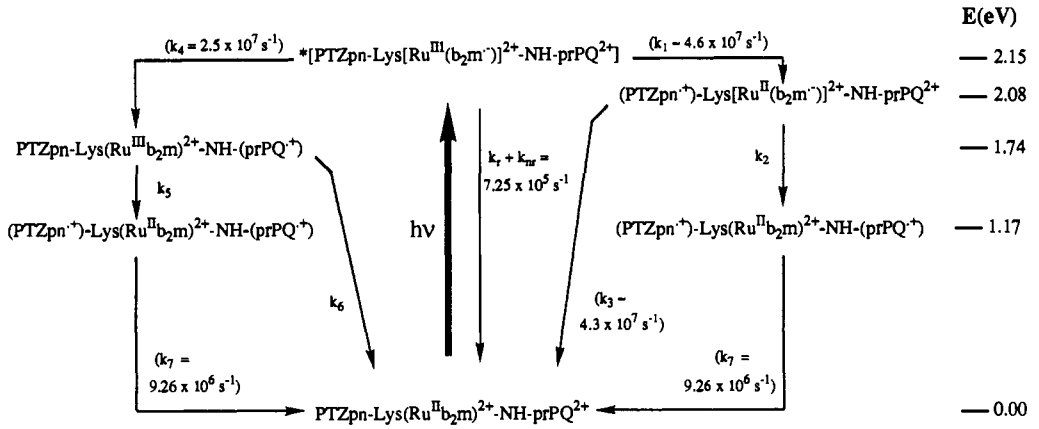

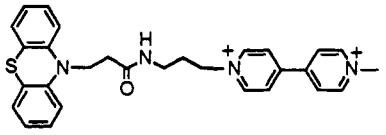

1 PTZpn-NH-prPQ^{2+}

3 mM benzoquinone (BQ). Formation of the redox-separated state of the triad was followed by electron transfer from the electron donor TMBD to PTZpn$^{\bullet+}$ ($k = 6 \times 10^9$ M^{-1} s^{-1}) and electron transfer from prPQ$^{\bullet+}$ to the acceptor BQ ($k = 1 \times 10^9$ M^{-1} s^{-1}), Scheme VI. The electron-transfer reactions, k_1 and k_2 in Scheme VI, followed pseudo-first-order kinetics and were observed by monitoring the loss of the absorption signal for PTZpn$^{\bullet+}$ at 510 nm in the reaction with TMBD and the loss of absorption by prPQ$^{\bullet+}$ at 605 nm in the reaction with BQ. In the net reaction, visible light was converted into the chemical redox energy of the transient products,[37,38] TMBD$^{\bullet+}$ and BQ$^{\bullet-}$ (eq 2).

$$\text{TMBD} + \text{BQ} \xrightarrow[\text{Triad 1}]{h\nu_{532\ nm}} \text{TMBD}^{\bullet+} + \text{BQ}^{\bullet-} \qquad \Delta G^\circ = 0.8\ \text{eV} \quad (2)$$

Discussion

Model Chromophore. Spectroscopic and electrochemical data (Tables I and II) show that the modified ruthenium chromophores [Ru^{II}b$_2$m-NHCH$_3$]$^{2+}$, **3**, and [Boc-Lys(Ru^{II}b$_2$m)$^{2+}$-OH], **4**, retain the essential ground-state and excited-state properties of the parent complex, [Ru^{II}(bpy)$_3$]$^{2+}$. Comparison of the photophysical properties of **3** and **4** shows that attachment of the chromophore to the amino acid lysine has only a slight effect on the photophysical properties. Assemblies that incorporate the chromophore **3** show no evidence of photodecomposition or photosubstitution as a result of the laser irradiations described here when monitored by UV–visible spectroscopy or by HPLC chromatography.[39] The photostability of the mixed-chelate chromophore **3** was quantitated by comparison of its photosubstitution properties with those for [Ru^{II}(bpy)$_3$]$^{2+}$ and found to be similar. For **3**, the quantum yield for photosubstitution is $\Phi_P = 0.030 \pm 0.003$, compared with $\Phi_P = 0.029 \pm 0.001$ for [Ru^{II}(bpy)$_3$]$^{2+}$ measured under the same conditions.[16] Earlier studies[16a,40] of ruthenium chromophores found that photosubstitution of a bipyridyl ligand can occur following MLCT excitation and thermally activated barrier crossing to low-lying ligand field (dd) states. The existence of slight ligand-loss photochemistry (photodecomposition) in **3** supports some contribution of dd states to the excited-state properties. The participation of dd states can also be probed by examination of the temperature dependence of the emission quantum yield. Data for **3** (Figure 2) show that there is a very small dependence of the relative emission intensity on temperature. From the absence of a significant temperature dependence of Φ_{em}, the population of dd states that does occur may happen during the relaxation processes that occur following MLCT excitation, rather than by thermal population as in [Ru^{II}(bpy)$_3$]$^{2+}$.[16a]

The emission lifetime of the excited state of chromophore **3** (τ_{em} = 1380 ns; $\Phi_{em} = 0.087 \pm 0.009$) is surprisingly long relative to [Ru^{II}(bpy)$_3$]$^{2+}$ (τ_{em} = 920 ns;[16b] $\Phi_{em} = 0.062 \pm 0.001$,[13a] all in CH$_3$CN at room temperature) given their relative emission energies, λ_{max} = 645 nm for **3** and λ_{max} = 626 nm for [Ru^{II}(bpy)$_3$]$^{2+}$, and the usual energy gap dependence on nonradiative decay usually observed for these complexes.[40,41] The difference in emission energies parallels the greater ease of reduction of m-NHCH$_3$ as an acceptor ligand relative to bpy (see below). The increase in lifetime is attributable, in part, to the absence of a significant contribution to nonradiative decay in **3** by thermal population and decay from a dd state, which in [Ru^{II}(bpy)$_3$]$^{2+}$ accounts for 26% of excited-state decay at room temperature.[40a]

Time-resolved resonance Raman spectroscopy has been successfully utilized to identify the ligand site where the electron resides in the excited state in various Ru^{II} mixed-chelate complexes.[16b,42] In [Ru^{II}(bpy)$_3$]$^{2+*}$, the transient Raman spectrum is comprised of bands for (bpy$^{\bullet-}$) with a less intense set of

(36) (a) Young, R. C.; Meyer, T. J.; Whitten, D. G. *J. Am. Chem. Soc.* **1975**, *97*, 4781. (b) Nagle, J. K.; Bernstein, J. S.; Young, R. C.; Meyer, T. J. *Inorg. Chem.* **1981**, *20*, 1760.

(37) Takemoto, K.; Matsusaka, H.; Nakayama, S.; Suzuki, K.; Ooshika, Y. *Bull. Chem. Soc. Jpn.* **1968**, *41*, 764.

(38) (a) Foster, R.; Thompson, T. J. *Trans. Faraday Soc.* **1962**, *58*, 860. (b) Slifkin, M. A. *Spectrochim. Acta* **1964**, *20*, 1543.

(39) Complexes which incorporate the electron donor phenothiazine exhibited slight decomposition upon exposure to light in the presence of oxygen. All such complexes were prepared, purified, and stored with the exclusion of light and oxygen to the extent possible. Irradiation of degassed samples, either freeze–pump–thawed or bubbled with Ar for > 10 min, resulted only in very minimal changes in their UV–visible absorption spectra. In the presence of both light and oxygen, oxidation at the sulfur of PTZ occurs, which eliminates the electron-donating ability of PTZ. The oxidized form of PTZ (probably a sulfoxide) has a very distinctive absorption feature, a shoulder in the 300-nm region, and thus is easily detected.

(40) (a) Caspar, J. V.; Meyer, T. J. *J. Am. Chem. Soc.* **1983**, *105*, 5583. (b) Barqawi, K. R.; Llobet, A.; Meyer, T. J. *J. Am. Chem. Soc.* **1988**, *110*, 7751. (c) Lumpkin, R. S.; Kober, E. M.; Worl, L. A.; Murtaza, Z.; Meyer, T. J. *J. Phys. Chem.* **1990**, *94*, 239.

(41) The vibrational overlap factors were calculated by using the room-temperature spectral fitting parameters. The values are essentially the same. For [Ru^{II}(b$_2$m-NHCH$_3$)]$^{2+}$, $\ln[F_{(calc)}] = -18.08$; for [Ru^{II}(bpy)$_3$]$^{2+}$, $\ln([F_{(calc)}] = -18.18$.

(42) (a) Wrighton, M. S.; Mabrouk, P. A. *Inorg. Chem.* **1986**, *25*, 526. (b) McClanahan, S. F.; Dallinger, R. F.; Holler, F. J.; Kincaid, J. R. *J. Am. Chem. Soc.* **1985**, *107*, 4853.

Scheme VI

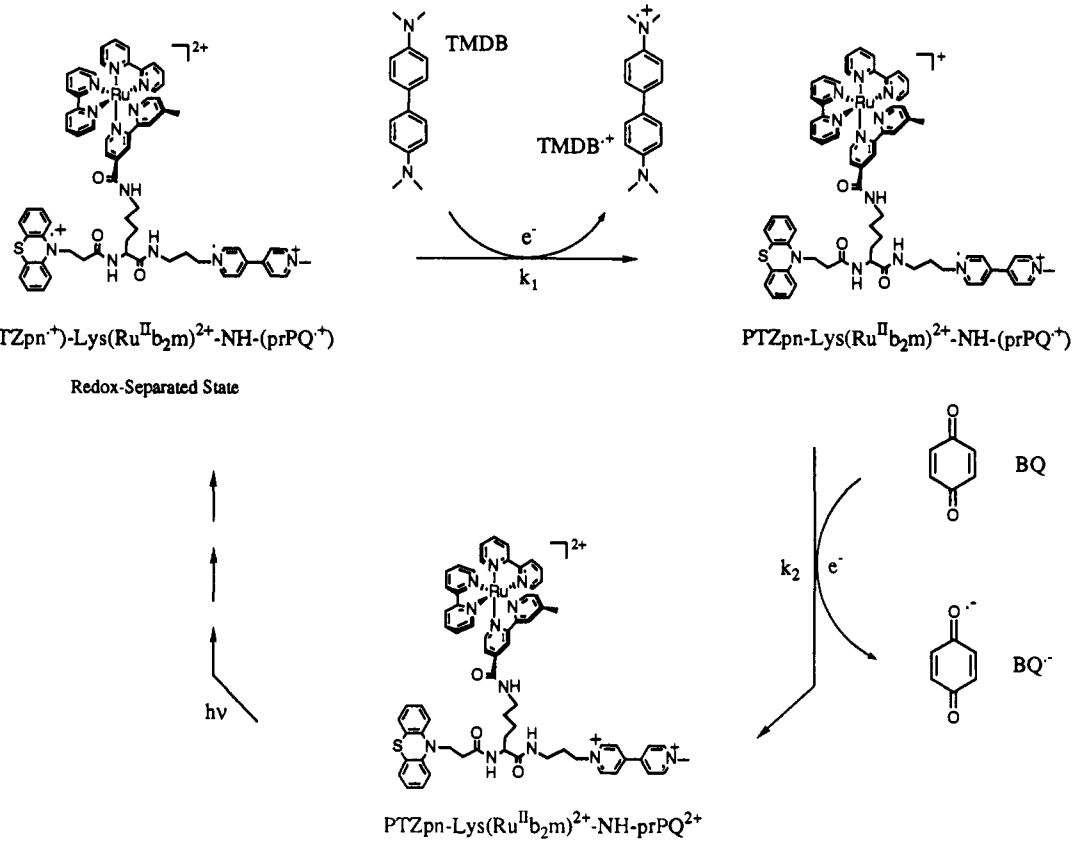

bands for bpy (i.e., in $[Ru^{III}(bpy^{\cdot-})(bpy)_2]^{2+}$).[25,43] With 354.7-nm laser excitation, the Raman bands of ($bpy^{\cdot-}$) are strongly enhanced in resonance with the excited-state (π,π^*) absorption near 360 nm, while the neutral bpy ligands are weakly enhanced by the ground-state (π,π^*) absorption near 320 nm.

The excited-state Raman spectrum of **3** (Figure 3) shows that following $d\pi \rightarrow \pi^*(bpy),\pi^*(m\text{-}NHCH_3)$ excitation, the excited electron resides primarily on m-$NHCH_3$. The -CH_3 and -$C(O)NHCH_3$ groups of m-$NHCH_3$ are electron donating and withdrawing, respectively, relative to -H. The net effect is to lower slightly the π^* level of m-$NHCH_3$ relative to unsubstituted bpy so that m-$NHCH_3$ becomes the primary acceptor ligand.[40b] This conclusion is also consistent with electrochemical measurements of the first reduction of **3** which occurs at −1.28 eV, while the first $bpy^{0/-}$ couple in $[Ru^{II}(bpy)_3]^{2+}$ occurs at −1.33 eV.[16b,44] Based on this energy difference, a $m^{\cdot-}/bpy^{\cdot-}$ ratio of ~8:1 would be expected. Neither $bpy^{\cdot-}$ nor ground-state m-$NHCH_3$ is observed in the transient Raman spectrum of **3**; the intensities of the bands are probably too small to be observed and/or may be hidden under the $m^{\cdot-}$ bands. Given the small difference in potentials for the $m^{0/-}$ and $bpy^{0/-}$ couples, $\Delta G°$ for intraligand electron transfer

$$[Ru^{III}b_2m^{\cdot-}]^{2+} \rightarrow [Ru^{III}bb^{\cdot-}m]^{2+}$$

is probably small and positive, with the excited electron localized primarily on m-$NHCH_3$.

Chromophore–Quencher Dyads. The directly linked dyads $[(Ru^{II}b_2m)^{2+}\text{-}NH\text{-}prPQ^{2+}]$, **5**, and $[(Ru^{II}b_2m)^{2+}\text{-}NH\text{-}prPTZ]$, **6**, were constructed to explore excited-state electron transfer in amide-based chromophore–quencher complexes. In the donor–chromophore dyad **5**, quenching by forward electron transfer from ($b_2m^{\cdot-}$) to ($prPQ^{2+}$) occurs with $\Delta G° \sim -0.44$ eV, and $k_f > 2.5 \times 10^8$ s^{-1} (Scheme I). A value for the reorganizational energy λ of 0.50 eV can be calculated from the self-exchange rate constants for the $bpy^{0/-}$ and $PQ^{2+/+}$ couples.[45a,b] From the rapid rate constant for the quenching step it can be inferred that the -$NH\text{-}(CH_2)_3$- bridge between the chromophore and the electron acceptor is sufficiently flexible to allow a close-contact encounter. Back electron transfer between $PQ^{\cdot+}$ and Ru^{III} occurs very rapidly, $k_b > k_f$, in the inverted region with $\Delta G° \sim -1.71$ eV and $\lambda = 0.89$ eV[45b,c] and may be facilitated by significant through-space electronic coupling between $prPQ^{\cdot+}$ and Ru^{III}.

Excited-state quenching of the acceptor–chromophore dyad **6** occurs by electron transfer from PTZpn to Ru^{III} in the normal region with $\Delta G° \sim -0.18$ eV and reorganizational energy $\lambda \sim 0.91$ eV.[45c,d] Back electron transfer between ($b_2m^{\cdot-}$) and ($PTZpn^{\cdot+}$) occurs in the inverted region with $\Delta G° \sim -1.97$ eV and $\lambda \sim 0.37$ eV.[45a,d] The decay of the resulting redox-separated state occurs in 33 ns, $k_b = 3 \times 10^7$ s^{-1} (Scheme II). The influence of side-chain conformation may also appear in the relatively rapid rate constants for back electron transfer in dyad **6**. Close contact and relatively strong electronic coupling could lead to enhanced electron-transfer rate constants here as well as in dyad **5**.

The preparation of the tripeptide $[(Ru^{II}b_2m)^{2+}$-Ala-Lys-(PTZpn)-Ala-OH], **7**, was an intermediate stage in the design and construction of more complex assemblies. Our overall strategy is to select redox modules from a pool of various donors, acceptors, and chromophores, and to assemble them in designed combinations

(43) (a) Dallinger, R. F.; Woodruff, W. H. *J. Am. Chem. Soc.* **1979**, *101*, 4391. (b) Bradley, P. G.; Kress, N.; Hornberger, B. A.; Dallinger, R. F.; Woodruff, W. H. *J. Am. Chem. Soc.* **1981**, *103*, 7441.

(44) (a) Hammett values[44b] are also consistent with this conclusion, and have been correlated previously with bipyridine electrochemical potentials.[44c] For CH_3, $\sigma_p = -0.14$; H, $\sigma_p = 0$; and $CONHCH_3$, $\sigma_p = 0.36$; these are values[44b] which show that the net effect of the two substituents on m-$NHCH_3$ is electron withdrawing. (b) Exner, O. In *Correlation Analysis in Chemistry: Recent Advances*; Chapman, N. G., Shorter, J., Eds.; Plenum: New York, 1978; pp 439–450. (c) Hino, J. K.; Della Ciana, L.; Dressik, W. J.; Sullivan, B. P. *Inorg. Chem.* **1992**, *31*, 1072.

(45) For the calculation of λ from k_{ex}, see, for example: Chen, P.; Duesing, R.; Graff, D. K.; Meyer, T. J. *J. Phys. Chem.* **1991**, *95*, 5850. Self-exchange rate constants at 298 K appear: (a) $b^{0/-}$ in CH_3CN in Reynolds, W. L. *J. Phys. Chem.* **1963**, *67*, 2866. (b) $PQ^{2+/+}$ in CH_3OH in Dai, S. Ph.D. Dissertation, University of Tennessee, 1990; private communication from Prof. F. Williams, University of Tennessee. (c) $[Ru(bpy)_3]^{3+/2+}$ in CD_3CN in Chan, M.-S.; Wahl, A. C.; *J. Phys. Chem.* **1978**, *82*, 2542. (d) $PTZ^{+/0}$ in CH_3CN in Kowert, B. A.; Marcoux, L.; Bard, A. J. *J. Am. Chem. Soc.* **1972**, *94*, 5538.

by forming amide links between the modules to yield multifunctional amino acids and peptides. Since the most expeditious method of preparing oligopeptides is by the Merrifield technique of solid-phase peptide synthesis,[34] it was necessary to determine at an early stage if the redox modules chosen were amenable to assembly by means of this technique. The synthesis of the tripeptide **7** was designed to investigate this point. This peptide has the same redox-active components as the dyad **6** but has greater conformational flexibility. The lifetime for the redox-separated state of 39 ns for **7** (as compared to 33 ns for **6**) suggests that both **6** and **7** attain conformations that have similar donor–chromophore separation distances at which back electron transfer occurs.

We began the assembly of multiple redox-active sites on a lysine scaffold starting with the chromophore–quencher dyads **8** and **9**. These dyads were prepared both for comparison with the simple amide-linked compounds described above and to serve as direct models for a more complex triad assembly. Upon excitation, the donor–chromophore dyad **8** gave rise to a redox-separated state, $[(PTZpn^{\bullet+})\text{-}Lys(Ru^{II}b_2m^{\bullet-})^{+}\text{-}OCH_3]$, with a 23-ns lifetime. This value is similar to but slightly smaller than the redox-separated state lifetime observed for the analogous dyad **6** and may reflect the greater conformational flexibility of the phenothiazine donor relative to the ruthenium amide chromophore in **8**, where they are separated by eleven atoms, as opposed to **6**, where the two are separated by only five atoms.

Dyad **9** exhibits the same qualitative behavior as chromophore–acceptor complex **5**. Efficient quenching of the initial MLCT state is followed by very rapid back electron transfer to the ground state in both cases, so that the redox-separated state, $[\text{Boc-Lys-}(Ru^{III}b_2m)^{3+}\text{-NH-prPQ}^{\bullet+}]$, does not build up in sufficient concentration to be observed. However, in **9**, the quenching rate constant is significantly slower, with MLCT quenching occurring with $k = 2.5 \times 10^7\ s^{-1}$ (τ = 40 ns). This relatively slow rate constant may also be attributable to the greater conformational flexibility of the lysine system **9**, but in this case the quencher may tend to be farther away from the chromophore, which results in slower forward electron transfer. Electrostatic repulsion between the two positively charged redox centers may also play a role in the conformational dynamics in both **5** and **9**.

The observations described for the donor–chromophore PTZ dyads **6**, **7**, and **8** are consistent with previous observations[46] of electron transfer following MLCT excitation of the complexes $[Ru^{II}(bpy)_2(bpy\text{-}(CH_2)_n\text{-PTZ})]^{2+}$ with n = 1 or 4.

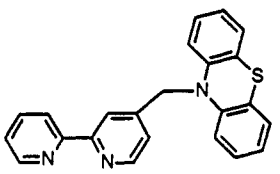

bpy-(CH_2)-PTZ

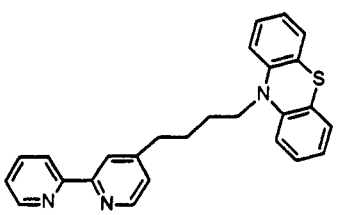

bpy-$(CH_2)_4$-PTZ

In the case of n = 4, the donor PTZ is tethered to the metal center by a flexible methylene chain, analogous to structures **6–8**, and the redox-separated state lifetime was τ_{rs} = 22 ns for $[Ru^{II}(bpy)(bpy^{\bullet-})(bpy\text{-}(CH_2)_4\text{-}PTZ^{\bullet+})]^{2+}$ in CH_3CN. This is similar to the lifetimes of 23–29 ns observed for the dyads **6–8**.

(46) Danielson, E. W., unpublished results.

In contrast, τ_{rs} = 125 ns for the n = 1 case. In this complex, PTZ is connected to the chromophore by a one-carbon link which does not permit it to fold closely to the metal center and thus back electron transfer is not facilitated by enhanced donor–acceptor electronic coupling. These observations support a through-space mechanism for back electron transfer in which the conformational mobility of the donor has a controlling effect on the back electron-transfer rate and thus on the redox-separated state lifetime. This also emphasizes the importance of developing systems which incorporate more rigid supporting frameworks or where spacers exist between the redox sites to achieve longer redox-separated state lifetimes.

The redox-separated states that involve $Ru^{III}/PQ^{\bullet+}$ in the dyads **5** and **9** are not directly observed by transient absorption spectroscopy. This is consistent with data previously reported[47a] for related ruthenium complexes in which paraquat was attached to a substituted bipyridine by a one- or two-methylene spacer. In all cases, the ^{3}MLCT quenching rates observed[47a] by picosecond transient absorption spectroscopy were very short, on the order of 40–200 ps, and for $[Ru^{II}(bpy)_2(bpy\text{-}(CH_2)_2\text{-}PQ^{2+}]$, it was found that $k_f < k_b$, with $k_f = 5.3 \times 10^9\ s^{-1}$ (τ = 188 ps) and $k_b = 7.5 \times 10^9\ s^{-1}$ (τ = 133 ps). The ligand bpy-$(CH_2)_2$-PQ^{2+} is shown below. Similar observations were made for a series of related

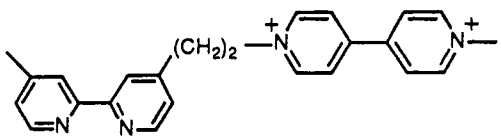

bpy-$(CH_2)_2$-PQ^{2+}

cases with n = 2, where it was found that $k_f < k_b$ as we report for our systems. Decay by back electron transfer occurred in 75–140 ps over a 200-mV $\Delta G°$ range centered at −1.5 eV. Studies of related ruthenium(bpy-diquat) systems reported similar findings of back electron transfer rates that were faster than forward electron-transfer rates.[47b,c]

The distinctive differences observed in redox-separated state lifetimes for the PTZ dyads and the PQ^{2+} dyads in spite of their similar geometrical arrangement is very interesting. The difference in rate constants is most likely a direct consequence of Marcus inverted-region behavior. Back electron transfer for the PTZ system lies much more deeply in the inverted region and thus occurs more slowly. The driving force in the PTZ systems is approximately 0.340 eV more favorable, and the quantity ($\Delta G° + \lambda$) is −0.860 eV further in the inverted region than for the PQ^{2+} systems. The PTZ redox-separated state returns to the ground state by back electron transfer from $m^{\bullet-}$ to $PTZ^{\bullet+}$, a $\pi^* \rightarrow \pi$ transfer that occurs on the nanosecond time scale. In the PQ^{2+} case the redox-separated state returns to the ground state by back-electron transfer from $PQ^{\bullet+}$ to Ru^{III}, a $\pi^* \rightarrow d\pi$ transfer that occurs very rapidly. The difference in orbital composition may also have an effect on the relative rate constants.

Chromophore–Quencher Triad. The assembly of multiple redox-active sites on an amino acid scaffold was continued with the preparation of the lysine-based donor–chromophore–acceptor triad **1**, $[\text{PTZpn-Lys}(Ru^{II}b_2m)^{2+}\text{-NH-prPQ}^{2+}]$. This triad incorporates both the electron-transfer donor phenothiazine and the acceptor paraquat. It was designed to provide greater spatial separation of the oxidized and reduced redox equivalents, which should increase both the redox-separated state lifetime and the efficiency of its formation upon photolysis.

(47) (a) Yonemoto, E. H.; Riley, R. L.; Kim, Y. I.; Atherton, S. J.; Schmehl, R. H.; Mallouk, T. E. *J. Am. Chem. Soc.* **1992**, *114*, 8081. (b) Ryu, C. K.; Wang, R.; Schmehl, R. H.; Ferrere, S.; Ludwikow, M.; Merkert, J. W.; Headford, C. E. L.; Elliott, C. M. *J. Am. Chem. Soc.* **1992**, *114*, 430. (c) Schmehl, R. H.; Ryu, C. K.; Elliott, C. M.; Headford, C. E. L.; Ferrere, S. *Adv. Chem. Ser.* **1989**, *228*, 211. (d) Cooley, L. F.; Headford, C. E. L.; Elliott, C. M.; Kelley, D. F. *J. Am. Chem. Soc.* **1988**, *110*, 6673.

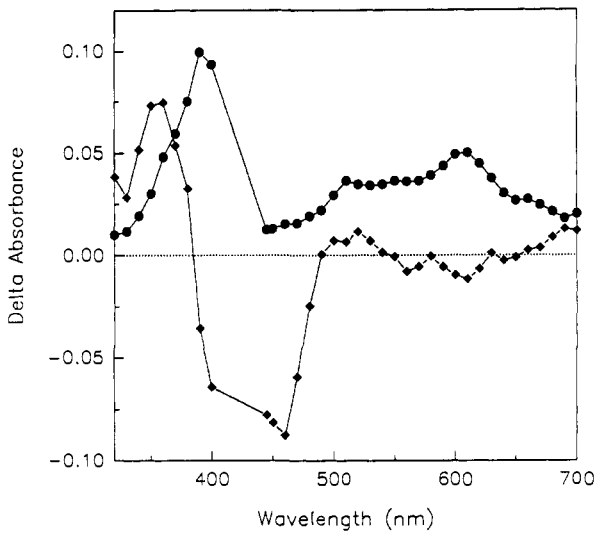

Figure 8. Components of the transient spectrum extracted by global analysis of the nanosecond full transient absorption spectrum of **1**. The filled diamonds show the first component and correspond to the transient spectrum of the ^{3}MLCT excited state. The filled circles are the second component detected in the analysis and correspond to the transient absorption of the redox separated state of **1**, composed of PTZpn$^{\bullet+}$ and prPQ$^{\bullet+}$.

Triad **1** exhibited efficient (>95%) quenching of the MLCT excited state upon excitation, where the initial step for quenching of the MLCT excited state ($k = 7.1 \times 10^7$ s^{-1}) was taken from the rate constant for the recovery of the MLCT bleach at 460 nm, which coincided with the rate of appearance of the transient absorptions of the redox-separated state. Quenching gave rise to the anticipated redox-separated state, [(PTZpn$^{\bullet+}$)-Lys-(Ru^{II}b$_2$m)$^{2+}$-NH-(prPQ$^{\bullet+}$)], which had a lifetime of 108 ns ($k = 9.26 \times 10^6$ s^{-1}) in CH_3CN as detected by nanosecond transient absorption measurements of the decay of the transient absorption signals for PTZpn$^{\bullet+}$ and PQ$^{\bullet+}$. Values for these rate constants were obtained by global analysis of the entire nanosecond transient absorption spectrum. The same value for the quenching rate constant was obtained from both nanosecond and picosecond measurements. The nanosecond transient absorption spectrum was rigorously reproduced by a biexponential function and the kinetic analysis detected two contributing (colored) states besides the ground state in the nanosecond transient spectra. The transient absorption difference spectra of the two states extracted by the fitting program are shown in Figure 8. The first corresponds to the absorption spectrum of the ^{3}MLCT excited state, [PTZ-pn-Lys*(Ru^{III}b$_2$m$^{\bullet-}$)$^{2+}$-NH-prPQ^{2+}] (diamonds), while the second corresponds to the redox-separated state, [(PTZpn$^{\bullet+}$)-Lys-(Ru^{II}b$_2$m)$^{2+}$-NH-(prPQ$^{\bullet+}$)] (circles). The analysis did not detect PTZpn$^{\bullet+}$ and prPQ$^{\bullet+}$ separately, which indicates that the secondary electron-transfer step(s) that follow initial quenching and lead to the final redox-separated state are rapid, compared to the initial quenching event.

The progression of the series of picosecond transient spectra in the time domain (Figure 4) clearly shows that the bleaching of the MLCT absorption (the 460-nm feature) is rapid, occurring within the 25-ps laser pulse, and that recovery of the bleach is correlated in time with the appearance of the redox-separated state. This is further illustrated in Figure 5, which shows a normalized plot of ΔA vs time for three selected wavelengths. Figure 5 shows that the growths of the signals at 510 and 605 nm occur with the same rate constant, $k = 7.24 \times 10^7$ s^{-1} (τ = 13.8 ns). This value is within experimental error of the value obtained by global analysis of the nanosecond transient absorption data. The recovery of the bleach monitored at 430 nm is also shown in Figure 5 and occurs with the same rate constant. This result is consistent with a mechanism in which formation of the MLCT excited state is followed by two electron-transfer steps that occur in rapid succession and result in formation of the redox-separated state. Formation of the redox-separated state by the alternate mechanism of direct excitation of a charge-transfer complex between the donor PTZpn and the acceptor prPQ^{2+} is not consistent with these spectral observations.

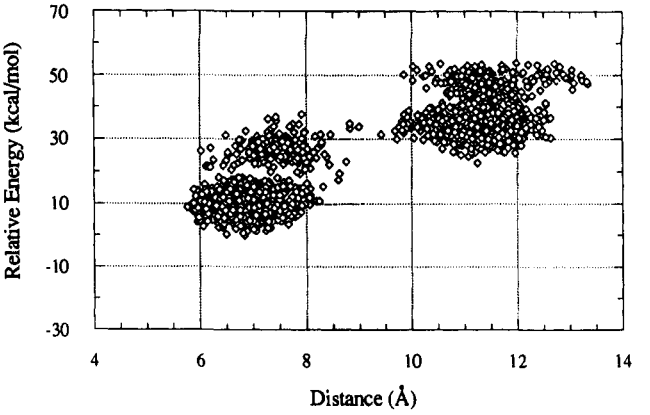

Figure 9. Distribution plot of relative energy vs distance (Å) of edge-to-edge separation between PTZ and PQ^{2+} in triad **1**. Note that the folded conformations (separation distance of 6–8 Å) have somewhat lower energy than more extended conformations (distances of 10.5–12.5 Å).

The appearance of exponential decay kinetics in triad **1** and the other assemblies indicates that the relative orientations of the attached redox sites have an important effect on the rate constants for electron transfer. In all cases, these sites are tethered together by relatively flexible side chains. There are a variety of possible orientations, some more important than others, based on the rotational conformations of these links. The observation of single-exponential decay kinetics implies either that interconversions between conformers are rapid relative to an electron transfer that occurs from a single, readily accessible conformation of the triad or that electron transfer may occur from a series of equilibrated conformers, whose rate constants are too close to deconvolute. A less likely possibility is that a single (presumably close contact) conformation of the triad predominates in solution and electron transfer occurs from this conformation. According to dynamic modeling[48] of the triad **1**, the donor, PTZpn, and the acceptor, prPQ^{2+}, are separated by a minimum of ~4 Å and a maximum of ~13 Å (edge to edge, Figure 9). The triad resides primarily in two conformation sets, one with an average PTZpn/prPQ^{2+} separation of ~7 Å and the other, at slightly higher energy, with an average separation distance of ~11 Å. Selected conformations obtained from the dynamics calculation are shown in Figure 10; it must be noted that the calculation does not consider either solvent or counterions for **1**, which has a total charge of +4. In Figure 10A, an extended conformation is shown. Either of the two quenchers can fold in and stack with one of the bpy ligands, in close contact with the metal center as in Figure 10B. The second quencher can also fold in to form a triple π-stacked structure (Figure 10C,D gives two views of the same structure). The quenchers can stack with either PTZ or PQ^{2+} in the central position. Based on the apparent degree of flexibility of **1** and its model compounds, the back electron-transfer reaction, k_7, probably occurs through space. There is no basis for effective through-bond electronic coupling over the ~16 Å through-bond distance between the donor and the acceptor.

A sequence of events that may occur following excitation of triad **1** is illustrated in Scheme V. As shown in the Scheme, excitation of **1** gives rise to the ^{3}MLCT excited state of the

(48) Distances were calculated beginning with a structure minimized by the conjugate gradient technique. The Biosym software DISCOVER was used for the dynamics calculation with a 100-fs equilibration. The calculation was conducted at 300 K over 117 110 steps, where 1 step = 1 fs. A CVFF89 force field was used for the dynamic analysis. Note that neither solvent nor counterions were taken into account in this calculation.

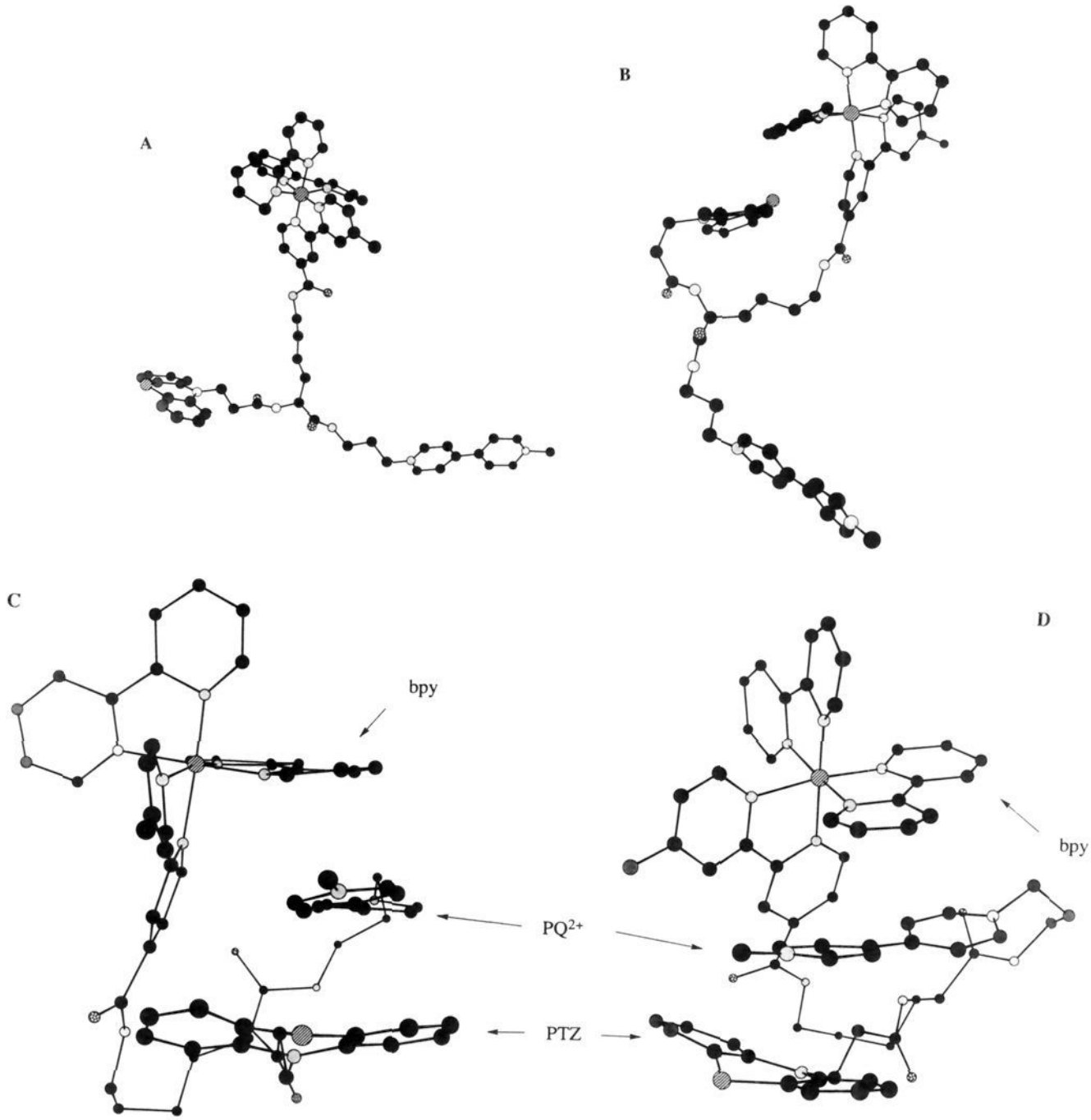

Figure 10. Selected conformations of triad **1** obtained from the dynamics calculation:[48] (A) an extended conformation; (B) a partially folded conformation in which PTZ is stacked beneath one of the bpy ligands of the chromophore; (C) a folded conformation in which PQ^{2+} is stacked between PTZ and bpy; and (D) a rotated view of the same structure shown in (C). The hydrogen atoms are not displayed. Note that either PQ^{2+} or PTZ can fold into the central position.

chromophore, *[PTZpn-Lys[($Ru^{III}b_2m^{\bullet-}$)]$^{2+}$-NH-$prPQ^{2+}$]. Along the right-hand branch of the scheme, initial reductive quenching by PTZ (k_1) to form [($PTZpn^{\bullet+}$)-Lys[($Ru^{II}b_2m^{\bullet-}$)]$^{+}$-NH-$prPQ^{2+}$] can be followed by either redox-separated state formation (k_2) or return to ground state (k_3). In the left-hand branch of the scheme, initial oxidative quenching by PQ^{2+} (k_4) to form [PTZpn-Lys[($Ru^{III}b_2m$)]$^{3+}$-NH-($prPQ^{\bullet+}$)] can be followed by either redox-separated state formation (k_5) or return to the ground-state (k_6). The redox-separated state [($PTZpn^{\bullet+}$)-Lys[(Ru^{II}-b_2m)]$^{2+}$-NH-($prPQ^{\bullet+}$)] decays back to the ground state by electron transfer from -($prPQ^{\bullet+}$) to ($PTZpn^{\bullet+}$)- (k_7). The rate constants given in Scheme V and their derivations are summarized in Table III and described in the following paragraphs.

The value for $k_r + k_{nr}$ was obtained from the study of complex **3** that established the photophysical properties of the unquenched chromophore. The lifetime of **3**, $\tau_{em} = 1380$ ns, gives an estimate for $k_{obs} = 1/\tau_{em} = k_r + k_{nr} = 7.26 \times 10^5\ s^{-1}$ for the MLCT excited state in the absence of electron-transfer quenching. Use of the

Table III. Rate Constants for Scheme V

rate constant	value (s^{-1})	derived from
$k_r + k_{nr}$	7.26×10^5	emission lifetime of model chromophore **3**
k_{obs}	7.1×10^7	direct measurement of quenching in triad **1**
k_1	2.4×10^7	calculated from Φ_{rsa}, k_{obs}, k_2, and k_3
k_2	$\geq 2 \times 10^{10}$	estimated from the picosecond study on triad **1**
k_3	4.3×10^7	redox-separated state lifetime of model dyad **8**
k_4	4.6×10^7	calculated from $k_{obs} = k_1 + k_4 + k_r + k_{nr}$
k_5	$\geq 2 \times 10^{10}$	estimated from the picosecond study on triad **1**
k_6	$\gg k_4$	nanosecond and picosecond study of model dyad **9**
k_7	9.26×10^6	direct measurement of redox-separated state decay of triad **1**

emission quantum yield for **3**, $\Phi_{em} = 0.087 = k_r/(k_r + k_{nr}) = k_r\tau_{em}$, permits calculations of $k_r = 6.31 \times 10^4\ s^{-1}$ and $k_{nr} = 6.61 \times 10^5\ s^{-1}$. The equation $[1 - (\Phi_{em(1)}/\Phi_{em(3)})] = 0.95$, in which $\Phi_{em(n)}$ is the emission quantum yield for compound **n**, establishes the efficiency of MLCT quenching in the chromophore/quencher complex **1** at 95% relative to the model chromophore **3**.

The initial quenching step, $k_{obs} = 7.1 \times 10^7\ s^{-1}$ ($\tau_{obs} = 14$ ns) where $k_{obs} = k_1 + k_4 + k_r + k_{nr}$, was taken from the rate constant for the recovery of the MLCT bleach at 460 nm, which coincided with the rate of appearance of the transient absorptions of the redox-separated state. The redox-separated state lifetime, $k_7 = 9.26 \times 10^6\ s^{-1}$ ($\tau_{rs} = 108$ ns), represents the decay of the transient absorption signals for $PTZpn^{\bullet+}$ and $prPQ^{\bullet+}$. Both k_{obs} and k_7 were obtained from direct measurements on **1** as described above.

The appearance of $prPQ^{\bullet+}$ in the redox-separated state of the triad occurs with a rate constant indistinguishable from that for the appearance of $PTZpn^{\bullet+}$, even when monitored on the picosecond time scale (see Figure 5). This implies that k_2 (and k_5) are rapid, on the order of $\geq 2 \times 10^{10}\ s^{-1}$. A slower rate would be distinguishable in this experiment by the observation of an intermediate state resulting from k_1 (or k_4).

The redox-separated state of the PTZ dyad **8**, [(PTZ-$pn^{\bullet+}$)-Lys($Ru^{II}b_2m^{\bullet-}$)$^+$-OCH_3] has a lifetime of 23 ns ($k_{b(\text{Scheme III})} = 4.3 \times 10^7\ s^{-1}$) which provides the estimate for k_3 in Scheme V. There was no evidence for $prPQ^{\bullet+}$ in transient absorption difference spectra of **9**, even though the MLCT emission was efficiently quenched, from which we conclude that $k_6 \gg k_4$ in Scheme V. We are unable to estimate the relative values of k_6 and k_5, although both are likely $> 1 \times 10^{10}\ s^{-1}$ based on the previous studies[47] described above for k_6 and the picosecond experiments for k_5.

The redox-separated state was produced with an efficiency Φ_{rs} of 0.34 and stored 1.17 V of energy based on the measured redox potentials of the donor and acceptor components. From the high degree of emission quenching, initial electron transfer quenching is rapid and efficient. The less-than-unit redox-separated state formation efficiency must have its origin in the deactivational processes, k_3 and/or k_6 in Scheme V. Based on the behavior of the paraquat model dyads **5** and **9**, we might make the assumption that decay by k_4 is only followed by k_6 and therefore no redox separated state results from initial oxidative quenching. All of the redox-separated state [(PTZ$pn^{\bullet+}$)-Lys($Ru^{II}b_2m$)$^{2+}$-NH-($prPQ^{\bullet+}$)] would then arise from k_1 followed by k_2. If we take the direct observations of $\Phi_{rs} = 0.34$ and $k_{obs} = 7.1 \times 10^7\ s^{-1}$, the model chromophore value for $k_r + k_{nr} = 7.25 \times 10^5\ s^{-1}$, the model dyad **8** value for k_3 of $4.3 \times 10^7\ s^{-1}$, and estimate a value for k_2 of $2 \times 10^{10}\ s^{-1}$ based on the picosecond data, k_1 can be calculated from the redox-separated state quantum yield by $\Phi_{rs} = (k_1/k_{obs})\cdot[k_2/(k_2 + k_3)]$. This gives $k_1 = 2.4 \times 10^7\ s^{-1}$. Use of $k_{obs} = k_1 + k_4 + k_r + k_{nr}$ gives $k_4 = 4.6 \times 10^7\ s^{-1}$. In this analysis, the major loss of efficiency in redox-separated state formation is the k_4–k_6 pathway since k_3 is too slow to contribute significantly to the decay of [(PTZ$pn^{\bullet+}$)-Lys($Ru^{II}b_2m^{\bullet-}$)$^+$-NH-($prPQ^{2+}$)]. Although consistent with the experimental data, the major uncertainty in this analysis is the validity of the assumption that quenching by k_4 does not give rise to redox-separated state. The basis for the assumption is the behavior observed in the models **5** and **9**, which do not give rise to observable redox-separated states. However, it is certainly possible that k_5 is rapid enough to compete with k_6. Note that the values calculated for k_1 and k_4 differ from the quenching rate constants for the model dyads **8** and **9**, but only by a factor of 2–3.[49]

The validity of this analysis is strengthened by the results of the conformational analysis of **1** described above. If one accepts the assumption that electron-transfer quenching occurs primarily from closest contact conformations, the observed and calculated rate constants given in Scheme V can be understood based on the availability of various conformations such as those shown in Figure 10B–D. As in outer-sphere electron transfer, the advantage of close contact is in the maximization of electronic coupling and minimization of solvent reorganization.[50] Through-bond electron transfer may also play a role in these systems but to a limited degree because of the saturated chemical links that connect the electron transfer sites.[51]

If oxidative quenching by PQ^{2+} (k_4) occurs first from a conformation in which PQ^{2+} is close to the metal center (similar to Figure 10B), it is possible (likely) that the resulting species would decay rapidly by back-electron transfer to Ru^{III} (k_6). This is observed in the paraquat model dyad **9**. Back electron transfer could occur before a conformational shift could make quenching by PTZ possible (k_5), or before electron transfer over the longer Ru^{III}-PTZ separation distance shown in the conformation in Figure 10C. On the other hand, if PTZ were stacked closest to the metal center so that reductive quenching occurs first (k_1), it is known from the behavior of the PTZ model dyad **8** that this redox-separated state is able to persist for a significant length of time. Conformational motion would permit the second electron transfer to PQ^{2+} (k_2), or there would be an extended period for the second electron transfer to occur over the longer distance of a triple-stacked conformation. The observation of a relatively long redox-separated state lifetime (k_7) might indicate that the electron transfers that give rise to redox-separated state occur from a succession of conformations like Figure 10B where first PTZ folds close to the metal center to undergo electron transfer and then extends as PQ^{2+} folds in to undergo the second electron transfer, in conformational equilibrium with extended conformations such as Figure 10A. The triple-stacked conformations such as Figure 10C,D may or may not play an important role in back electron transfer.

The lifetime of the redox-separated state of triad **1**, 108 ns ($k_7 = 9.26 \times 10^6\ s^{-1}$), is considerably larger than that of the redox-separated state of the PTZ dyad **8**, [(PTZ$pn^{\bullet+}$)-Lys-($Ru^{II}b_2m^{\bullet-}$)$^+$-OCH_3], for which $\tau_{rs} = 23$ ns ($k_{b(\text{Scheme III})} = k_{3(\text{Scheme V})} = 4.3 \times 10^7\ s^{-1}$). The addition of the second electron-transfer quencher in triad **1** results in nearly a 5-fold increase in the redox-separated state lifetime even though back electron transfer for **8** is further in the inverted region with $(\Delta G^\circ + \lambda) = -1.72$ eV while $(\Delta G^\circ + \lambda) = -0.4$ eV for **1**. Both electron transfers occur in the inverted region, but the conformational requirements are different. The decrease in k for **1** may be associated with an important contribution from the conformational reorganization required to reach a stacked structure such as that in Figure 10C,D.

It was demonstrated that the energy harvested by triad **1** and stored in its redox-separated state can be utilized further by conversion into chemical redox energy. As shown in Scheme VI, formation of the redox-separated state of **1** in the presence of the secondary electron donor, TMBD, and acceptor, BQ, was followed by chemical electron transfers that returned **1** to its ground state and gave rise to the oxidized and reduced products, $TMBD^{\bullet+}$ and

(49) The kinetic model that we favor is described in the text; it is self-consistent and accounts for the experimental data. However, in such a complex system, there are other kinetic models consistent with the observations. For example, if the redox-separated state is produced from both quenching pathways k_1 and k_4, the identical single-exponential rise-time kinetics observed for $PTZ^{\bullet+}$ and $PQ^{\bullet+}$ by picosecond spectroscopy of **1** would require that $k_1 \approx k_4 \approx 3.5 \times 10^7\ s^{-1}$, and therefore that half of the observed redox-separated state would result from each quenching branch. Beginning with this assumption, and taking $k_2 = k_5 = 2 \times 10^{10}\ s^{-1}$, we calculate that $k_3 = k_6 = 3.8 \times 10^{10}\ s^{-1}$ to account for a yield of 0.34. This model accounts for the experimental result, but there is neither direct evidence nor compelling reason to assume equal quenching by both reductive and oxidative pathways, and model results are not consistent with identical rates for k_3 and k_6. As another possibility, if we assume the model value for k_4 of $2.5 \times 10^7\ s^{-1}$, that all redox-separated state arises from $k_1 \rightarrow k_2$, and that $k_2 = 2 \times 10^{10}\ s^{-1}$, then we calculate $k_1 = 4.5 \times 10^7\ s^{-1}$, and $k_3 = 1.7 \times 10^{10}\ s^{-1}$. In this analysis, the quenching rate constants k_1 and k_4 parallel those of the models **8** and **9**, but the decay rate constant k_3 is considerably more rapid than the value for the model dyad **8**.

(50) (a) Sutin, N. *Prog. Inorg. Chem.* **1983**, *30*, 441. (b) Marcus, R. A.; Sutin, N. *Biochim. Biophys. Acta* **1985**, *811*, 265.

(51) (a) Bowler, B. E.; Raphael, A. L.; Gray, H. B. *Prog. Inorg. Chem.* **1990**, *38*, 259. (b) Chen, P.; Duesing, R.; Graff, D. K.; Meyer, T. J. *J. Phys. Chem.* **1991**, *95*, 5850.

$BQ^{\bullet-}$. These underwent back electron transfer on a longer time scale. This demonstrates that the redox-separated state of **1** persists long enough to undergo useful secondary redox chemistry and that the stored energy of the state may be harvested by simple electron transfer reactions.[36c,52]

We are pursuing the assembly of more complex redox-active peptides by using redox modules such as those described here.

Acknowledgments are made to the National Science Foundation (Grant CHE-8806664), the National Institute of General Medical Sciences (Grants GM32296 and GM42031), and the North Carolina Biotechnology Center (Grant 8913-ARIG-0104) for support of this research. This investigation was also supported by the National Institute of General Medical Sciences, National Research Service Award GM14511 to S. L. Mecklenburg. Special acknowledgment is made to Dr. David Thompson for many helpful discussions.

(52) (a) Bock, C. R.; Meyer, T. J.; Whitten, D. G. *J. Am. Chem. Soc.* **1974**, *96*, 4710. (b) Bock, C. R.; Meyer, T. J.; Whitten, D. G. *J. Am. Chem. Soc.* **1975**, *97*, 2909. (c) Delaive, P. J.; Lee, J. T.; Abruña, H.; Sprintschnik, H. W.; Meyer, T. J.; Whitten, D. G. *Adv. Chem. Ser.* **1978**, *168*, 28.